JOURNAL OF BIOMOLECULAR STRUCTURE AND DYNAMICS
https://doi.org/10.1080/07391102.2020.1852117

Taylor & Francis
Taylor & Francis Group

Virtual screening of phytoconstituents from miracle herb *nigella sativa* targeting nucleocapsid protein and papain-like protease of SARS-CoV-2 for COVID-19 treatment

Sahabjada Siddiqui[a], Shivbrat Upadhyay[a], Rumana Ahmad[b], Anamika Gupta[b], Aditi Srivastava[b], Anchal Trivedi[b], Ishrat Husain[b], Bilal Ahmad[c], Maqusood Ahamed[d] and Mohsin Ali Khan[e]

[a]Deparment of Biotechnology, Era's Lucknow Medical College and Hospital, Era University, Lucknow, Uttar Pradesh, India; [b]Department of Biochemistry, Era's Lucknow Medical College and Hospital, Era University, Lucknow, Uttar Pradesh, India; [c]Research Cell, Era's Lucknow Medical College and Hospital, Era University, Lucknow, Uttar Pradesh, India; [d]King Abdullah Institute for Nanotechnology, King Saud University, Riyadh, Saudi Arabia; [e]Chancellor, Era's Lucknow Medical College and Hospital, Era University, Lucknow, Uttar Pradesh, India

Communicated by Ramaswamy H. Sarma

ABSTRACT

Severe acute respiratory syndrome coronavirus 2 (SARS-CoV-2) is a novel etiological agent of coronavirus disease 2019 (COVID-19). *Nigella sativa*, commonly known as black seed or black cumin, has been a historical and traditional plant since thousands of years. Based on their therapeutic efficacy, the chief components of terpenoids and flavonoids were selected from *N. sativa* seeds and seed oil. This study was designed to check the antiviral efficacy of *N. sativa* main phytoconstituents against five potential targets of SARS-CoV-2 using *in silico* structure-based virtual screening approach. Out of twenty five phytocomponents, ten components showed best binding affinity against two viral proteins *viz.* N-terminal RNA binding domain (NRBD; PDB ID: 6M3M) of nucleocapsid protein and papain-like protease (PL_{-PRO}; PDB ID: 6W9C) of SARS-CoV-2 using AutoDock 4.2.6, AutoDock Vina and iGEMDOCK. PASS analyses of all ten phytocomponents using Lipinski's Rule of five showed promising results. Further, druglikeness and toxicity assessment using OSIRIS Data Warrior v5.2.1 software exhibited the feasibility of phytocomponents as drug candidates with no predicted toxicity. Molecular dynamics simulation study of NRBD of SARS-CoV-2 nucleocapsid protein-alpha-spinasterol complex and PL_{-PRO}-cycloeucalenol complex displayed strong stability at 300 K. Both these complexes exhibited constant root mean square deviation (RMSDs) of protein side chains and Cα atoms throughout the simulation run time. Interestingly, PL_{-PRO} and NRBD are key proteins in viral replication, host cell immune evasion and viral assembly. Thus, NRBD and PL_{-PRO} have the potential to serve as therapeutic targets for *N. sativa* phytoconstituents in drug discovery process against COVID-19.

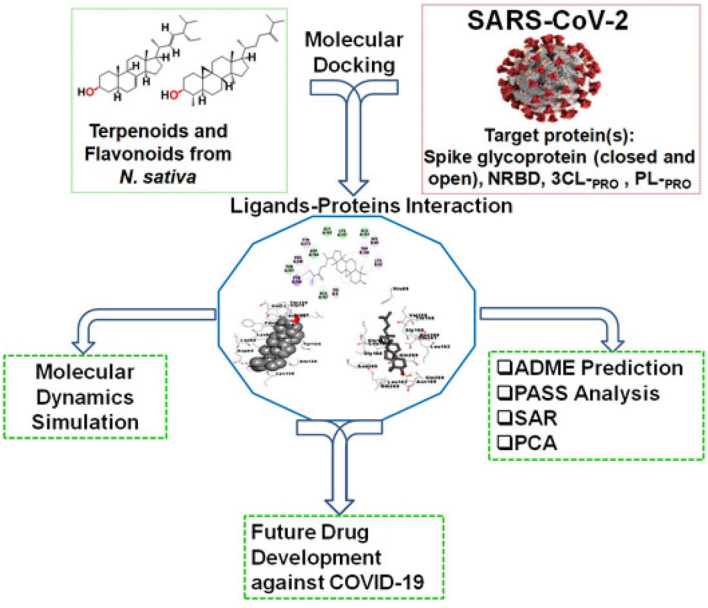

ARTICLE HISTORY
Received 17 July 2020
Accepted 11 November 2020

KEYWORDS
Nigella sativa; phytocomponents; SARS-CoV-2; nucleocapsid protein; papain-like protease; molecular chemoinformatics

CONTACT Rumana Ahmad rumana_ahmad@yahoo.co.in; rahmad@erauniversity.in Department of Biochemistry, Era's Lucknow, Medical College & Hospital, Era University, Lucknow, Uttar Pradesh, 226003, India

Supplemental data for this article can be accessed online at https://doi.org/10.1080/07391102.2020.1852117

Abbreviations: ADMET: Absorption, Distribution, Metabolism, Excretion and Toxicity; BE: Binding energy; COVID-19: Coronavirus disease 2019; K_d: Dissociation constant; MD: Molecular Dynamics; NRBD: N-terminal RNA binding domain; PCA: Principal component analysis; PL-$_{PRO}$: Papain-like protease; 3CL-$_{PRO}$: 3C-like protease; SAR: Structure-activity relationship; RMSD: Root mean square deviation; RMSF: Root mean square fluctuation; SARS-CoV-2: Severe acute respiratory syndrome coronavirus 2

1. Introduction

Coronavirus disease 2019 (COVID-19) is a highly contagious disease caused by severe acute respiratory syndrome coronavirus 2 (SARS-CoV-2). It was first identified in December 2019 in Wuhan city of China and has spread globally, thereafter, resulting in the ongoing pandemic (Riou & Althaus, 2020). COVID-19 has spread rapidly in the human population and has caused a high number of deaths globally. According to Center for Disease Control and Prevention, human coronaviruses cause mild to severe infections in humans. But this new virus SARS-CoV2 is a public concern because not much is known about its spread amongst the people and its mechanism of function in the human body.

SARS-CoV-2 is an enveloped positive-sense and single-stranded RNA genome containing virus belonging to Coronaviridae family of β- viruses (Pal et al., 2020). SARS-CoV-2 has shown similarity with severe acute respiratory syndrome (SARS) and Middle East respiratory syndrome (MERS) viruses. Coronaviruses possess four structural proteins namely spike-S, envelope-E, membrane-M and nucleocapsid-N proteins. The entry of coronavirus into host cells is mediated by the transmembrane S glycoprotein (Li, 2016). S protein contains two functional subunits *viz.* S1 responsible for binding to the host cell receptor and S2 for fusion of the viral and host membranes which allow the CoV-RNA genome to enter inside the host cells. N-terminal domain (NTD) and C-terminal domain (CTD) are the major structural and functional domains of the nucleocapsid protein, which regulate the replication and transcription of viral RNA. The most important function of the NTD of nucleocapsid protein is RNA binding, while the primary job of the CTD is dimerization (Chang et al., 2016; Walls et al., 2020). Open reading frame (ORF) of CoV RNA genome encodes two large polyproteins PP1a and PP1ab. After processing of PPs by cysteine proteases, 16 non-structural proteins (NSPs) are formed. The C-terminal ends of these PPs are cleaved by chymotrypsin-like cysteine protease (3CL-$_{PRO}$) and the N-terminal end is processed by the papain-like protease (PL-$_{PRO}$). The PL-$_{PRO}$ cleaves the N-terminal region of the PPs to generate three NSPs which help in the formation of replicase transcriptase complex for viral propagation (Prajapat et al., 2020). Thus, both NTD of nucleocapsid protein and PL-$_{PRO}$ represent important targets from the perspective of drug discovery.

The incidence of COVID-19 has elevated intense attention not only in India but worldwide. No specific therapeutic is available till date and, therefore, to control the propagation of COVID-19, current management including travel restrictions, social distancing, lockdown, patient isolation and supportive medical care are being used by the governments of pandemic-hit countries. Considering the proportion of the disastrous epidemic, research is being carried out at a breakneck speed, so that future treatment schemes with effective novel therapeutic agents and vaccines can be released immediately. In some countries, anti-HIV and antimalarial drugs are being used as prophylaxis, but these drugs lack the desired biological effects and are not free from adverse effects in clinical trials. Hydroxychloroquine is an antimalarial drug and in case of viral infection, it increases the pH within intracellular vacuoles to inhibit the replication of different viruses by interfering with endosome/lysosome trafficking or viral protein maturation during virion maturation; while, ivermectin is a broad spectrum anti-parasitic drug that paralyzes and kills the parasites (Choudhary & Sharma, 2020). Ivermectin is known to exert its antiviral effect by preventing viral proteins moving in and out of the host cell's nucleus, which is essential for replication of coronavirus (Caly et al., 2020). Among the repurposed drugs for COVID-19, hydroxychloroquine has been approved by the FDA as an Emergency Use Authorization (EUA) against COVID-19, while ivermectin is an FDA-approved antiparasitic agent with antiviral activity against a broad range of viruses, such as influenza, human immunodeficiency virus (HIV), dengue virus, West Nile virus, and Venezuelan equine encephalitis virus (Choudhary & Sharma, 2020; Heidary & Gharebaghi, 2020). Previous studies have also reported the antiviral effects of hydroxychloroquine and ivermectin against several distinct negative-sense single-strand RNA viruses, including SARS-CoV-2 (Choudhary & Sharma, 2020; Liu et al., 2020). Therefore, hydroxychloroquine and ivermectin are expected to inhibit viral load in patients with COVID-19.

Development of novel drugs is also a time consuming process with an exorbitant cost. Therefore, a planned and systematic approach is needed for rational drug design and discovery to overcome the burden of the pandemic. Bioinformatics has been an integral part of drug development in this age of personalized medicine and cost-effective public health outcomes. In the post genomic era, virtual *in silico* prediction of promising drug candidates outsourced from the plant kingdom can play a significant role in drug discovery in complementary and alternative medicine, thus proving to be time and cost effective. Medicinal plants and their phytoconstituents offer diverse pharmacological properties and unlimited scope as part of Indian traditional system of medicine *i.e.* Ayurveda; however, most of them remain to be studied as therapeutic agents against the ongoing pandemic.

Nigella sativa, belonging to family Ranunculaceae , is commonly known as black seed or black cumin. In historical and religious texts, *N. sativa* is known as a miracle curative herb for all ailments, except death (Yimer et al., 2019). The black seed is used for stimulating the body's energy and helping recovery from fatigue and dispiritedness (Ahmad et al.,

2004). *N. sativa* seeds and oils have wide therapeutic effects against many ailments such as skin diseases, jaundice, gastrointestinal problems, anorexia, conjunctivitis, dyspepsia, rheumatism, diabetes, hypertension, intrinsic hemorrhage, paralysis, amenorrhea, anorexia, asthma, cough, bronchitis, headache, fever, influenza, eczema and cancer (Forouzanfar et al., 2014, Ahmad et al., 2013, Ahmad, Khan, et al., 2020; Yarnell & Abascal, 2011). The seeds and oil of *N. sativa* contain terpenoids, flavonoids, phenolics, alkaloids, saturated and unsaturated fatty acids (Forouzanfar et al., 2014; Menounos et al., 1986; Yarnell & Abascal, 2011). Because of the rich nutraceuticals in *N. sativa,* it could be extensively used to prevent and cure COVID-19. Till date, only limited studies have reported the antiviral activities of *N. sativa* showing protective effect of black seed oil against murine cytomegalovirus infection (Salem & Hossain, 2000) and *in silico* antiviral activity of some unsaturated/saturated fatty acids against angiotensin-converting enzyme 2 (ACE2) receptor of host cells (Ahmad, Abbasi, et al., 2020). However, none of the studies has reported the antiviral activities of selected terpenoids and flavonoids (Table 1) against SARS-CoV-2 viral proteins *viz.* NTD of nucleocapsid protein and PLpro of SARS-CoV-2 by employing chemoinformatics tools.

In the present study, twenty five phytoconstituents from *N. sativa* were selected for their binding affinity with five target proteins of SARS-CoV-2 using AutoDock, of which ten showed best binding kinetics against viral N-terminal RNA binding domain (NRBD) of nucleocapsid protein and papain-like protease (PL-$_{PRO}$). MD simulation study of two bound ligand-protein complexes exhibited strong stability while all phytoconstituents displayed druglikeness with no predicted toxicity. Our present findings are further supported by the previously reported antiviral efficacies of a class of terpenoids and flavonoids (Ghildiyal et al., 2020; Naithani et al., 2010; Yang et al., 2020). Thus, NRBD and PL-$_{PRO}$ of SARS-CoV-2 warrant further validation as potential drug targets through wet lab and clinical studies.

2. Materials and methods

2.1. Data sources

The present study was carried out at Molecular Chemoinformatics Section, Cell and Tissue Culture Lab, Dept. of Biochemistry, Era's Lucknow Medical College and Hospital, Era University, Lucknow. A total number of twenty five bioactive components of black cumin (*Nigella sativa*) were selected from Dr. Duke's Phytochemical and Ethnobotanical Databases (https://phytochem.nal.usda.gov/phytochem/search/list), comprising thirteen compounds from seed oil and twelve compounds from *N. sativa* seeds (Table S1). The criteria for selection were based on their respective structure-activity relationships and prospective targeted metabolic pathways. During compound screening, all ubiquitous chemicals were excluded and phytochemicals belonging to the class of terpenoids and flavonoids were selected for the present study. The compounds from seed oil used in the present study were 24-methylene-cycloartanol (CID_94204), Alpha-spinasterol, also known as spinasterol (CID_5281331), arachidonic-acid (CID_444899), beta-amyrin (CID_73145), beta-sitosterol (CID_222284), campesterol (CID_173183), citrostadienol also known as alpha-1-sitosterol (CID_9548595), cycloartenol (CID_92110), cycloeucalenol (CID_101690), taraxerol (CID_92097), thymol(CID_6989), thymoquinone (CID_10281), and tirucallol (CID_101257). The selected phytochemicals from seed source were astragalin (CID_5282102), carvone (CID_7439), D-limonene (CID_440917), nigellicine (CID_11402337), nigellidine (CID_136828302), nigellimine, also known as isosalsolidine (CID_20725), nigellimine-n-oxide (CID_348288664), nigelline, also known as damascenine (CID_21368), nigellone, also known as dithymoquinone (CID_398941), quercetin-3-glucoside, also known as isoquercetin (CID_5280804), rutin (CID_5280805), and thymohydroquinone, also known as thymoquinol (CID_95779). Among the repurposed drugs for COVID-19, hydroxychloroquine and ivermectin are the mainstay for COVID-19 treatment in the present scenario. Though hydroxychloroquine is generally considered safe and side-effects are generally mild with no secondary or associated complications, it has been found to be toxic in SARS-CoV-2 patients with cardiovascular disorders (Touret & de Lamballerie, 2020). As far as ivermectin is concerned, huge uncertainty remains about whether this treatment can be safely and effectively repurposed to tackle the coronavirus. The major concern in using ivermectin as a repurposed drug against COVID-19 is the safety of its use in pregnant females and children below the age of 14. Whereas ivermectin generally does not cause problematic side effects at the currently used doses, there is still limited information about whether much larger doses would also be safe. Therefore, there is a need for better alternatives/substitutes for both these drugs; hence the premise of the current study. Thus, the standard drugs hydroxychloroquine (CID_3652) and ivermectin (CID_6321424) were also included in the present study for comparison of their physicochemical and drug properties with those of the selected *N. sativa* phytoconstituents.

2.2. Preparation of ligands

All phytochemicals of *N. sativa* belonging to the class of terpenoids and flavonoids were selected for ligand preparation. PubChem (https://pubchem.ncbi.nlm.nih.gov/) database was used to download 3D structures of all phytochemicals and reference drugs in .sdf format. Before docking, energy minimization of ligands was performed by ChemBio3D Ultra 14.0, with Force Field type MM2 and saved in .pdb format (Ahmad, 2019).

2.3. Preparation of target proteins/macromolecules

The 3D crystal structures of selected SARS-CoV-2 protein targets *viz.* spike glycoprotein (closed state, PDB ID: 6VXX), spike glycoprotein (open state, PDB ID: 6VYB), N-terminal RNA binding domain of nucleocapsid protein (NRBD, PDB ID: 6M3M), 3 C-like protease (3CL-$_{PRO}$ main protease, PDB ID: 6M03), and papain-like protease (PL-$_{PRO}$, PDB ID: 6W9C) whose X-ray diffraction structures are available in RCSB database, were downloaded from Protein Data Bank (http://www.rcsb.org/pdb) in .pdb format. Before docking analyses, all 3D

Table 1. List of ten bioactive components from *N. sativa,* standard drugs hydroxychloroquine and ivermectin and their respective binding to nucleocapsid protein (PDB ID: 6M3M) and papain-like protease (PL_{-PRO}, PDB ID: 6W9C) of SARS-CoV-2.

S. No.	Ligands	PDB: ID (SARS-CoV-2)	MF and MW of phyto-components	Molecular Structure	Pub Chem CID	Chemical Class of Ligands	Source
1.	24-methylene-cycloartanol	6M3M 6W9C	MF: $C_{31}H_{52}O$ MW: 440.7	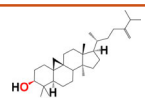	94204	Pentacyclic triterpenoid	Seed oil
2.	Alpha-spinasterol (spinasterol)	6M3M 6W9C	MF: $C_{29}H_{48}O$ MW: 412.7	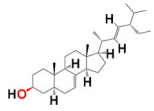	5281331	Steroid	Seed/seed oil
3.	Beta-amyrin	6W9C	MF: $C_{30}H_{50}O$ MW: 426.7	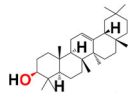	73145	Pentacyclic triterpenoid	Seed oil
4.	Beta-sitosterol	6M3M 6W9C	MF: $C_{29}H_{50}O$ MW: 414.7	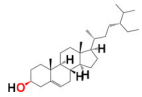	222284	Phytosterol	Seed oil
5.	Campesterol	6M3M 6W9C	MF: $C_{28}H_{48}O$ MW: 400.7	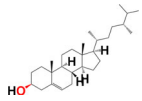	173183	Phytosterols	Seed/seed oil
6.	Citrostadienol (alpha1-sitosterol)	6M3M 6W9C	MF: $C_{30}H_{50}O$ MW: 426.7	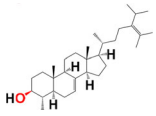	9548595	Sterol	Seed oil
7.	Cycloartenol	6W9C	MF: $C_{30}H_{50}O$ MW: 426.7	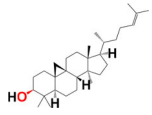	92110	Pentacyclic triterpenoid	Seed oil
8.	Cycloeucalenol	6M3M 6W9C	MF: $C_{30}H_{50}O$ MW: 426.7	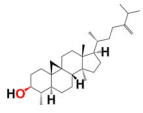	101690	Pentacyclic triterpenoid	Seed oil
9.	Taraxerol	6M3M 6W9C	MF: $C_{30}H_{50}O$ MW: 426.7	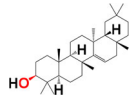	92097	Pentacyclic triterpenoid	Seed oil
10.	Tirucallol	6W9C	MF: $C_{30}H_{50}O$ MW: 426.7	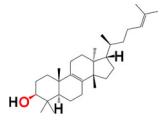	101257	Tetracyclic triterpene	Seed oil
11.	Hydroxy-chloroquine	6M3M 6W9C	MF: $C_{18}H_{26}ClN_3O$ MW: 335.9	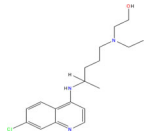	3652	4-aminoquinoline (Standard drug)	Chemotherapeutic agent
12.	Ivermectin	6M3M 6W9C	MF: $C_{48}H_{74}O_{14}$ MW: 875.1	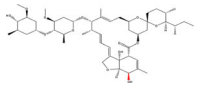	6321424	Macrocyclic lactone (Standard drug)	Derived from *Streptomyces avermitilis*.

protein structures were subjected to refinements and energy minimizations. Whole pdb structures of proteins were used for molecular docking study. The refinement procedure was carried out by addition of missing atoms to the residues, addition of polar hydrogen atoms and Kollman charges, removal of crystallographic water-molecules and external and irrelevant ligands and ions from the protein. During the docking period, the ligands were considered to be flexible and the proteins were considered as rigid. The highest binding energy (most negative) obtained for a ligand was considered as the ligand having maximum binding affinity to a particular target protein.

2.4. Molecular Docking analysis

2.4.1. AutoDock 4.2.6

Molecular docking of selected twenty five phytoconstituents and two standard drugs against five target receptors/proteins of SARS-CoV-2 was performed using AutoDock version 4.2.6 (Morris et al., 1998). Autogrid was used to determine the position of the native ligand on the binding site of protein using grid spacing 0.375 Å and grid coordinates (X, Y and Z) axes at $60 \times 60 \times 60$. Lamarckian genetic algorithm (GA) parameter was employed using 10 runs of the GA criteria and the binding energies of the results were further analyzed (Oprea et al., 2001). After evaluating binding of twenty five phytochemicals with five proteins with AutoDock 4.2.6 software, ten phytochemicals and corresponding two target proteins were selected based on the lowest binding energy *i.e.* maximum binding affinity for further validation through two additional docking softwares *viz.* AutoDock Vina and iGEMDOCK version 2.1 (Ahmad, 2019).

2.4.2. AutoDock Vina

Execution of AutoDock Vina is faster than AutoDock 4.2.6, which reduces the size of the conformational space, allowing it to be searched reliably and reduces the computational effort in predictions of binding pockets (Trott & Olson, 2010). AutoDock Vina was used to perform docking simulations, generating 10 conformations of ligand in complex with the receptor, which were finally ranked on the basis of binding energy. The resulting conformations were visualized in Accelrys Biovia Discovery Studio 2017 R2 (Biovia, San Diego, CA, USA).

2.4.3. iGEMDOCK

Target proteins and ligands were further docked with iGEMDOCK version 2.1. The genetic algorithm (GA) parameters, which guided the docking procedure, were set as follows: population size = 200, generations = 70, and number of solutions = 2. After generating a set of poses, the best fit was selected which represented the total binding energy in the form of hydrogen bond (HB), van der Waals forces (VDW), and electrostatic interactions (EI) (Yang & Chen, 2004).

2.5. Analysis and visualization of docked ligand-protein complexes

Based on the obtained lowest binding energy (B.E.) and dissociation constant (K_d), the best orientation (pose) of the ligand-protein interaction was selected for computational analysis and visualization of docking site using Accelrys Biovia Discovery Studio version 2017 R2.

2.6. Prediction of activity spectra for substances (PASS) analysis

PASS analysis program predicts biological activity spectrum of a compound under study based on its structure-activity relationship with a known chemical entity (Ahmad, 2019). In this study, PASS analysis was performed using various online and offline tools as detailed below.

2.6.1. Lipinski's rule of five

The druglikeness of ten phytochemicals of black cumin and two standard antiviral drugs was evaluated using Lipinski's rule of five (Lipinski, 2004). The parameters of druglikeness such as MW $\leq$500, logP $\leq$5, number of hydrogen bond donors (NOHNH) $\leq$5 and hydrogen bond acceptor sites (NON)$\leq$10, topological polar surface area (TPSA) ($\leq$140 Å^2), and number of rotatable bonds ($\leq$10) were determined. In the present study, druglikeness of phytochemicals was calculated using online tool Molinspiration (http://www.molinspiration.com/cgi-bin/properties) and was compared with that of standard reference drugs.

2.6.2. Toxicity potential assessment

Toxicity risk assessment gives an idea about the probable side effects of compounds that may be used for further processing in drug discovery and development. The prediction of different properties of molecules at an early stage is a vital step in drug discovery and development process. Drug-toxicity risk parameters such as druglikeness, mutagenicity, tumorigenicity, reproductive and irritant effects were analyzed by the OSIRIS Data Warrior v5.2.1 (Khan et al., 2018).

2.7. Bioactivity score (BAS) prediction

BAS values suggest a compound's overall ability to be a potent drug candidate. Molinspiration chemoinformatics, an online tool (https://www.molinspiration.com/cgi-bin/properties), was used to predict the drug scores of the prospective phytoconstituents with respect to several human receptors like GPCRs, ion channels, kinases, nuclear receptors, proteases and enzymes. As a general rule, the higher the bioactivity score, the greater is the probability of the compound being active (Proudfoot, 2002).

2.8. Pharmacokinetic (PK) parameters prediction

The ADMET (Absorption, Distribution, Metabolism, Excretion and Toxicity) properties of all components including standard drugs were predicted using online SwissADME software (http://www.swissadme.ch/). This software analyses the important pharmacokinetic properties of a compound like distribution *viz.* blood-brain barrier (BBB) and skin permeability (LogKp), and its metabolism in terms of it being a P-glycoprotein (P-gp) substrate, Cytochrome P450 *viz.* CYP1A2, CYP2C19, CYP2C9, CYP2D6, CYP3A4 inhibitor as well as its lipophilicity for plasma membrane absorption (Tian et al., 2015, Delaney, 2004).

2.9. Principal component analysis (PCA) of phytoconstituents and standard drugs

PCA is a mathematical method to summarize multidimensional datasets into two or three principal components (inter-correlated quantitative variables) that can be visualized graphically with minimal loss of information. The covariance and correlation matrix are calculated to scale the matrix in such a way that data with high variance are compressed with data having low variance. PCA was performed for defining and visualizing various multidimensional 'property spaces' by assigning dimensions to numerical descriptors of molecular structures of phytoconstituents and standard drugs *viz.* MW, % Absorption and TPSA using OSIRIS Data Warrior v5.2.1. The bar charts and 3D scatter plots of principal components were made to depict druglikeness of *N. sativa* phytoconstituents to standard drugs using OSIRIS Data Warrior v5.2.1 (Ahmad, 2019).

2.10. Molecular Dynamics (MD) simulation using ligand and receptor molecular dynamics (LARMD) online server

MD simulation is very valuable for understanding the dynamic behaviors of fast internal motions to slow conformational changes at different timescales or even protein folding processes of biological macromolecules. MD simulation is also used to study the effect of explicit solvent molecules on protein structure and stability to obtain time-averaged properties of the biomolecular system, such as density, conductivity and dipolar moment, as well as different thermodynamic parameters, including interaction energies and entropies (Hospital et al., 2015). Ligand and Receptor Molecular Dynamics (LARMD) server provides a user-friendly online protocol (http://chemyang.ccnu.edu.cn/ccb/server/LARMD/index.php/home/index) to investigate and visualize the molecular dynamic property of ligand-driven protein molecule. MD simulation of cycloeucalenol with papain-like protease ($PL\text{-}_{PRO}$) (PDB ID: 6W9C) and alpha-spinasterol with NRBD of nucleocapsid protein (PDB ID: 6M3M) were carried out using online server LARMD. Out of three computational modules namely Nor_mod, Int_mod and Str_mod, Int_mod of LARMD was used to investigate the fluctuation of the protein. The softwares CAVER3.0, AMBER16, MDTraj and Bio3d are integrated into these three modules. The plugins and softwares such as JSmol, Chart.js and MolScript are integrated to visualize and analyze the result on the Web page (de Oliveira & de Oliveira, 2020; Yang et al., 2019). In the LARMD protocol, the AMBER ff14SB force field and general AMBER force field (gaff) were used for amino acid residues and ligands, respectively. The enthalpy and the entropy were calculated by the MM/PB(GB)SA method and empirical method, respectively. The binding free energy (ΔG_{bind}) based on binding energy (ΔE_{bind}), salvation entropy ($-T\Delta S_{sol}$) and conformational entropy ($-\Delta TS_{conf}$) was calculated using following equation: $\Delta G_{bind} = \Delta E_{bind} - T\Delta S_{sol} - T\Delta S_{conf}$. For protein-ligand interactions and the contribution of each residue, the binding energy was decomposed per residue by using the decomposition module of the AMBER16 program. Various parameters such as root-mean-square deviation (RMSD), radius of gyration (Rg), fraction of native contacts Q (x) analysis, root mean square fluctuation (RMSF), B-factor, PCA, MM/PB(GB)SA for energy analysis, hydrogen bonds and decompose analysis were evaluated using LARMD online protocol (Bahar et al., 2010).

3. Results

3.1. Docking analysis of phytocomponents of N. sativa against targeted proteins of SARS-CoV-2

AutoDock v4.2.6 was used for docking study of twenty five phytochemicals of *N. sativa* against five targeted proteins of SARS-CoV-2 (Table S1, S2 and S3). Thus, total one hundred twenty five ($25 \times 5 = 125$) binding combinations were generated for the study of molecular docking analysis (Table S4). Based on the best binding energy and dissociation constant (K_d) of ligand-protein interactions with AutoDock v4.2.6 tool, out of twenty five phytocomponents, ten active components with their corresponding targeted protein receptors were selected for further validation through two additional docking tools *viz.* AutoDock Vina and iGEMDOCK v2.1 (Table 1). Tables 2 and 3 summarize the various binding energy parameters, dissociation constants (K_d) and interacting amino acid residues participating in the binding pocket of NRBD of nucleocapsid protein and $PL\text{-}_{PRO}$ of SARS-CoV-2 with six and ten active components of *N. sativa*, respectively *versus* standard drugs hydroxychloroquine and ivermectin through AutoDock v4.2.6, AutoDock Vina and iGEMDOCK v2.1 tools.

As is evident from Table 2, all 6 phytoconstituents and ivermectin exhibited potent binding affinity to NRBD of SARS-CoV-2 nucleocapsid protein. AutoDock v4.2.6 analyses revealed that binding affinities of the phytoconstituents with NRBD of SARS-CoV-2 decreased in the order alpha-spinasterol > beta-sitosterol > campesterol > taraxerol > citrostadienol > 24-methylene-cycloartanol. However, the binding affinity of alpha-spinasterol (BE = −9.54 kcal/mol, Kd = 101.42 nM) was found to be greater than standard drugs ivermectin (BE = −9.08 kcal/mol, Kd = 220.28 nM) and hydroxychloroquine (BE = −3.96 kcal/mol, K_d = 1.25 mM). Thus, both alpha-spinasterol and ivermectin displayed 1000000 x greater affinity than hydroxychloroquine. The results received further confirmation from analysis using AutoDock Vina and iGEMDOCK v2.1 tools (Table 2). On the other hand, the selected phytoconstituents of *N. sativa* also exhibited potent binding affinity to $PL\text{-}_{PRO}$ of SARS-CoV-2. AutoDock v4.2.6 analyses revealed that the binding affinities of the phytoconstituents with $PL\text{-}_{PRO}$ of SARS-CoV-2 decreased in the order campesterol > cycloeucalenol > alpha-spinasterol > taraxerol > beta-sitosterol > citrostadienol > beta-amyrin > tirucallol > cycloartenol > 24-methylene-cycloartanol (Table 3). Interestingly, campesterol exhibited a 1000x stronger binding to $PL\text{-}_{PRO}$ of SARS-CoV-2 (BE = −9.71 kcal/mol, K_d = 76.87 nM) as compared to standard drugs, hydroxychloroquine (BE = −5.93 kcal/mol, K_d = 44.86 μM) and Ivermectin (BE = −4.98 kcal/mol, K_d = 224.79 μM). However, none of the phytoconstituents was found to interact with the catalytic residues of $PL\text{-}_{PRO}$ *viz.* Cys112, His273, Asp287, Trp107, thereby suggesting the allosteric binding of the Nigella phytoconstituents to viral $PL\text{-}_{PRO}$ (Báez-Santos et al.,

Table 2. Docking interactions of active components of *N. sativa* with N-terminal RNA binding domain (NRBD) of SARS-CoV-2 nucleocapsid protein (PDB ID: 6M3M) *versus* standard drugs hydroxychloroquine and ivermectin.

AutoDock v4.2.6					AutoDock Vina			iGEMDOCK v2.1				
S.No	Ligands	BE (kcal/mol)	K_d	Interacting amino acids	BE (kcal/mol)	K_d	Interacting amino acids	T.E. (kcal/mol)	VDW	HB	EI	Interacting amino acids
1.	24-methylene-cycloartanol	−8.29	842.64 nM	Ala126,Ala135,Asn49, Asp129, Asp64,Gly125, Gly130, Ile131,Ile132, Lys128,Phe67, Trp109, Trp133,Tyr124,	−9.8	76.87 nM	Gln161,Gln84,Glu137 Gly164,Gly70,Ile75,Leu160, Leu162,Leu168, Pro163,Pro81,Ser79,Thr136, Thr161,Thr166,Thr167	−96.16	−91.43	−4.72	0	Arg69,Gln161,Gln84, Glu137,Glu165,Gly70,Leu160, Leu162,Leu16,Pro163,Pro81,Ser79, Ser80,Thr136,Thr166,Tyr173
2.	Alpha-spinasterol	−9.54	101.42 nM	Ala126,Ala135,Arg69,Asp64,Gln71, Gly130,Gly70,Ile131,Ile132, Leu65,Lys128,Lys66,Phe67,Pro68, Th136,Trp133,Tyr124Val134	−9.6	101.42 nM	Ala107,Asp108,Asp164,Glu161, Glu167,Gly163His89, Leu162,Lys157,Lys92,Pro248,Thr301, Trp108,Trp93,Tyr264,Tyr264,Tyr273	−91.33	−84.04	−7.29	0	Asn109,Gln269,Glu161,Gly160, His89Leu162,Thr158,Val159
3.	Beta-sitosterol	−8.69	426.43 nM	Ala35,Arg69,Asp64,Gln71,Gly130, Gly70,Ile132,Leu65,Lys128, Lys66,Phe67,Pro68,Thr136, Trp109,Trp133,Tyr124,Val134	−10.4	76.87 nM	Asn76,Gln161,Gln71,Gln84, Gly70Leu160,Leu162, Leu168,Leu57,Pro163,Pro81,Ser79, Thr136,Thr166,THr167,Tyr173	−88.19	−84.69	−3.5	0	Ala126,Arg69,Asn127,Asn155, Gly125,Gly70Ile131,Ile132, Lys128,Phe67,Pro68, Trp133,Tyr124
4.	Campesterol	−8.57	522.64 nM	Ala126,Ala135Arg69, Asn127Asp129, Gln71,Gly70,Ile131 ,Lys128,Lys66,Phe67,Pro68,Trp133, Tyr124,Val134	−9.8	76.87 nM	Asn76,Gln161,Gln71,Gln84, Glu137,Gly165,Gly70,Leu160, Leu162,Leu168,Pro163Pro81,Ser79, Thr136,Thr166,THr167Thr77,Tyr173	−93.83	−90.33	−3.5	0	Gln161,Gln164,Gln84,Glu137, Gly165,Gly70,Leu162,Pro81,Ser79, Thr136,Thr166,Thr167
5.	Citrostadienol	−8.43	663.45 nM	Ala126,Arg69Asn127,Asn49, Asp129,Gly125,Ile131,Ile132, Lys128,Phe67,Pro152, Thr50,Trp133,Tyr124	−8.9	259.96 nM	Ala156,Asn127Asn155,Asn76, Asn78,Asp145,Gln161, Ile158,Thr149,Thr50,Trp53,Val159	−80.13	−75.88	−4.24	0	Ala156,Ala157,Asn155Asp145, Glm161,Gly148,His146, Ile158,Thr149,Val159
6.	Taraxerol	−8.5	588.67 nM	Asn49,Asp129,Asp64, Gly130,Ile131Ile132, Leu65,Lys128Lys656Trp133,Tyr124	−12.1	76.87 nM	Gln161,Gln71Gln84,Glu137, Gly165,Gly70,Ile75,Leu160, Leu162,Leu168,Pro163,Pro74Thr136, Thr166,Thr167,Thr173	−96.11	−93.61	−2.5	0	Gln161,Gln71,Gln84,Glu137, Gly165,Gly70,Ile75Leu160, Leu162,Leu168,Pro163,Pro74, Thr136,Thr166,Tyr173
7.	Hydroxychloroquine	−3.96	1.25 mM	Ala126,Arg69,Asn49,Ile131,Ile132, Lys66Phe67,Thr50,Trp133,Tyr124	−6.7	588.67 nM	Arg150,Asn151,Asn155, Asn76Gly148,Ile147,Ile158, Ile75,The77,Thr149,Thr50,Trp53	−78.61	−75.11	−3.5	0	Ala156,Asn76,Asp145,Gln161, Gly148,His146,Ile147,Ile158, Ile75,Thr149,Thr77,Val159
8.	Ivermectin	−9.08	220.28 nM	Ala126,Arg89,Arg89,Asn127,Asn154, Asn155,Asn49,Asn76,Asn78,Asp64, Gly117,Gly125,Ile131, Ile132,Leu65Lys128, Lys66,Pro118,Thr50,Trp133,Trp53	−9.8	76.87 nM	Ala157,Ala174,Ala56,Arg108, Arg150,His60,Pro152, Thr55,Thr58,Tyr110Tyr173,Val159	−114.23	−96.98	−17.28	0	Ala126,Ala51,Arg89,Asn127, Asn154,Asn155,Asn49,Asp129, Asp129,Asp64,Gly130,Ile131, Ile132,Leu65,Lys128,Lys66, Pro118,Thr50,Trp133, Tyr110,Tyr112

Table 3. Docking interactions of active components of *N. sativa* with papain-like protease (PL_{-PRO}) of SARS-CoV-2 (PDB ID: 6W9C) *versus* standard antiviral drugs hydroxychloroquine and ivermectin.

		AutoDock v4.2.6			AutoDock Vina			iGEMDOCK v2.1				
S. No.	Ligands	BE (kcal/mol)	K_d	Interacting amino acids	BE (kcal/mol)	K_d	Interacting amino acids	T.E. (kcal/m ol)	VDW	HB	EI	Interacting amino acids
1.	24-methylene-cycloartanol	−8.32	800.77 nM	Asn109,Asn109,Cys270,Gln269,Gln269, Gln269,Glu161,Gly160Gly160, Gly161,His89,Leu162,Thr158,Val159	−9.6	101.42 nM	Ala107,Asp108,Asp164,Glu161, Glu167,Gly163His89,Leu162, Lys157,Lys92,Pro248,Thr301, Trp108,Trp93,Tyr264Tyr264,Tyr273	−84.63	−78.99	−5.64	0	Asn109,Gln269,Gly160, Gly161,Leu162,Thr158Val159
2.	Alpha-spinasterol	−9.41	126.53 nM	Asn109,Asn109,Asp108,Cys270,Cys270, Gln269,Gln269,Gln269,Glu161,Gly150, Gly160,His89Leu162,Leu162,Val159	−9.0	220.28 nM	Asn109,Asp108,Cys270, Gln269,Glu161, Gly160,Gly160,His89Leu162,Val159	−91.9152	−86.94	−4.97	0	Asn109,Cys270Gln269, Glu161,Gly160, Leu162,Thr158,Val159
3.	Beta-amyrin	−8.79	357.58 nM	Gln1005,Gln1010,Ile1013,Leu102, Leu763,The1006Thr100,Thr1009,Val1008	−9.8	76.87 nM	Asn109Gln269,Glu161,Gly160, Leu162,Thr158,Val159	−84.40	−80.90	−3.5	0	Ala107,Asn267,Asp108,Asp164, Glu161,Glu167,Gly163,His89Leu162, Lys157,Lys92,Trp106,TYr264,Tyr268
4.	Beta-sitosterol	−9.14	198.01 nM	Asn109Asn109,Asn109,Asp108Cys270, Cys270,Gln269,Gln269,Gln269,Glu161 ,Gly160,Gly160,His89,Leu162,Leu162,Val159	−9.0	220.28 nM	Asn109,Gln269,Glu161, Gly160,Gly160, His89,Leu162,Thr158,Val159	−98.20	−92.93	−5.27	0	Asn109,Cys270Gln269,Glu161,Gly160, Gly160,His89,Leu162,Leu162,Thr158
5.	Campesterol	−9.71	76.87 nM	Asn109,Asn109,Asn109,Asp108,Cys270Cys270, Gln269,Gln269,Gln269,Glu161,Gly160, Gly160,Leu162,Leu162,Leu162	−9.2	155.9 nM	Asn109,Cys270Gln269,Glu161, Gly160Gly160,His89,Leu162, Thr158,Val159	−96.65	−96.65	0	0	Asn109,Asp108,Gln269Glu161, Gly160,Gly160,His89,Leu162, Ser85,Thr158,Val159
6.	Citrostadienol	−8.98	259.96 nM	Asn109,Asn109,Asn109,Asp108,Cys270, Gln269,Gln269,Glu161Glu161,Gly160, His89,Leu162,Leu162,Leu162, Thr158,Val159,Val159	−9.5	101.42 nM	Ala107,Asn267,Asp108,Asp164, Glu161,Glu167,Gly266,His89,Leu162, Lys157,Lys92,Pro248Trp106, Trp93,Tyr264	−91.70	−86.45	−5.25	0	Ala86,Asn109Asp108,Glu161, Gly160,His89,Ser85,Thr158,Val159
7.	Cycloartenol	−8.74	389.61 nM	Asn109,Asn109,Cys270,Gln269,Gln269, Gln269,Glu161,Glu161,Gly160,His89, Leu162,Leu162,Thr158,Val159	−8.8	389.61 nM	Asn109,Asp108,Gln269, Glu161,Gly160,His89, Leu162,Thr158Val159,Val159	−85.32	−79.14	−2.17	0	Ala107,Asp108,Asp164,Glu161, Glu167,Gly163,His89,Leu162, Lys157,Lys92,Trp106,Tyr264
8.	Cycloeucalenol	−9.65	84.23 nM	Asn109,Asn109,Asp108,Cys270,Gln269, Gln269,Gln269,Glu161,Glu161,Gly160Gly160, Gly160,Leu162,Leu162,Leu162,Val159	−9.3	155.9 nM	Ala107,Asp108,Asp164, Glu161,Glu167,Gly163, His89,Leu162,Lys157, Lys92,Pro248Thr301, Trp106,Trp93,Tyr264,Tyr273	−102.07	−93.20	−8.86	0	Asn109,Asp108,Cys270, Gln269,Gln289Glu161, Gly160,Gly160,His89, Leu162,Val159
9.	Taraxerol	−9.29	155.9 nM	Asn109,Asn109,Asn109, Cys270,Gln269Gln269, Gln269,Glu161,Gly160, Gly160,His89,Leu162, Leu162,Thr158,Val159,Val159	−10.0	76.87 nM	Asn109,Cys270, Gln269,Glu161,Gly160, Gly160,Leu162,Thr158,Val159	−100.31	−90.34	−9.96	0	Asn109,Asp108,Gln269,Glu161, Gly160,Leu162,Thr158,Val159
10.	Tirucallol	−8.78	368.93 nM	Asn109,Asn109,Asn109, Asp108,Cys270,Gln269, Gln269,Gln269,Glu160,Glu161,Glu161, Gly160,Leu162,Leu162,Thr158Val159	−8.6	522.64 nM	Ala107,Asn267Asn267, Asp108,Asp164, Leu162,Leu289,Pro248, Trp106,Tyr264,Tyr268	−84.35	−81.07	−3.27	0	Asn109,Gln269Glu161,Gly160, Leu162,Thr158,Val159
11.	Hydroxychloroquine	−5.93	44.86 μM	Asn109,Asn109,Asn109,Gln269,Gln269, Gln269,Glu161,Glu161,Gly160, Gly160,Leu162,Leu162	−7.2	588.67 nM	Asn109,Gln269Glu161Gly160, Leu162	−80.88	−80.88	0	0	Asn109,Cys270Gln269,Glu161, Gly160,Gly160,Leu162
12.	Ivermectin	−4.98	224.79 μM	Asp108,Glu161,Glu161,Gly160,Gly160, His89Leu162,Thr158,Thr158, Thr158,Val159,Val159	−9.3	155.9 nM	Ala153,Ala39,Arg82,Asn156, Asn88,Asp76,Cys155,His73,Ile44, Leu36,Lys92Ser78,Thr74, Tyr154,Tyr171	−103.44	−82.27	−21.17	0	Asp108,ASP108,Glu161, Gly160,Gly160,His89,Ser85, Thr158,Val159,Val159

2015). The docking results obtained from AutoDock v4.2.6, AutoDock Vina and iGEMDOCK v2.1 tools were visualized in Discovery Studio showing prominent interactions between various amino acid residues. Tables 4 and 5 display the best docking poses of six and ten active components of *N. sativa*, respectively, with NRBD of nucleocapsid protein and PL-$_{PRO}$ of SARS-CoV-2, *versus* standard drugs hydroxychloroquine and ivermectin.

As far as interaction of cycloeucalenol with PL-$_{PRO}$ and alpha-spinasterol with NRBD is concerned, it is noteworthy that cycloeucalenol and alpha-spinasterol had almost similar binding sites on the two proteins as the two reference drugs *viz.* hydroxychloroquine and ivermectin. Differences in interacting amino acid residues in binding pockets are due to variations in the functional groups and basic chains of cycloeucalenol and alpha-spinasterol. This difference in SAR causes the variation in interacting amino acid residues. Binding studies of cycloeucalenol to PL-$_{PRO}$ and alpha-spinasterol to NRBD when compared with those of reference drugs hydroxychloroquine and ivermectin to the same proteins revealed that cycloeucalenol and alpha-spinasterol bind at or near the site where the reference drugs bind, albeit with greater affinity in both the cases (Tables 2 and 3).

3.2. PASS analysis of selected phytocomponents using Lipinski's rule of five

Lipinski's rule describes molecular properties of a compound which are important for lead optimization and selectivity of a potential orally active drug candidate in clinical applications. Table 6 shows the PASS analysis of all ten phytocomponents of *N. sativa versus* standard drugs hydroxychloroquine and ivermectin in terms of their physicochemical properties by applying Lipinski's rule of five. Generally, an orally active compound should have no more than one Lipinski's violation otherwise its bioavailability is compromised. Interestingly, all 10 phytoconstituents from *N. sativa* exhibited only 1 Lipinski's violation in comparison to hydroxychloroquine which did not show any Lipinski's violation. On the other hand, ivermectin displayed 3 violations of Lipinski's rule of five.

3.3. Druglikeness and toxicity potential assessment

Table 7 depicts druglikeness and toxicity calculations of *N. sativa* phytoconstituents *versus* standard drugs hydroxychloroquine and ivermectin by OSIRIS data warrior. The results indicated that phytocomponents 24-methylene-cycloartanol, alpha-spinasterol, beta-amyrin, beta-sitosterol, campesterol, cycloeucalenol and taraxerol are safe to use with no predicted toxicity. However, citrostadienol and cycloartenol displayed irritant effects, while tirucallol exhibited adverse effect on the reproductive system. Hydroxychloroquine showed mutagenic effect but ivermectin did not show any predicted toxicity. A positive value obtained for alpha-spinasterol in druglikeness evaluation indicated that this molecule predominantly contains fragments present in commercial drugs. As expected, both hydroxychloroquine and ivermectin exhibited positive scores for druglikeness (Table 7).

3.4. Bioactivity scores (BAS) of N. sativa phytoconstituents

The predicted BAS of all 10 phytoconstituents of *N. sativa* and their comparison with those of standard drugs are summarized in Table 8. As a general rule, a molecule having BAS >0.00 is most likely to possess considerable biological activities, while compounds having values between −0.50 and 0.00 are presumed to be moderately active and compounds having BAS < −0.50, are expected to be inactive. The results of the present study demonstrated that all *N. sativa* phytoconstituents are biologically active molecules because none of the phytoconstituents had bioactivity scores <-0.50. Thus, all *N. sativa* phytocomponents are capable of producing the physiological actions by multiple mechanisms after interacting with GPCR ligands, nuclear receptor ligands or by acting as inhibitors of proteases and other enzymes. All of the phytoconstituents displayed considerable activity as protease inhibitors as evident from their positive BAS of >0.00, except taraxerol which was found to be moderatively active as a protease inhibitor (BAS 0.00). Interestingly, most phytoconstituents showed potent binding to papain like protease of SARS-CoV-2 (PDB ID: 6W9C), thus supporting their role as potential viral protease inhibitors. On the other hand, ivermectin was predicted to be inactive as a protease inhibitor (BAS −1.89) and this was further validated with molecular docking analysis in which ivermectin exhibited 1000x less affinity for PL-$_{PRO}$ (K_d 224.79 μM) as compared to the *N. sativa* phytoconstituents which had their respective K_d with respect to SARS-CoV-2 PL-$_{PRO}$ in nM (Table 3). A similar trend was seen for the behavior of *N. sativa* phytoconstituents as nuclear receptor ligands (NRLs). All of them displayed positive BAS scores >0.00, which means they are expected to be considerably active as NRLs. The results were in agreement with the obtained docking scores for *N. sativa* phytoconstituents which had their respective K_d with respect to NRBD of SARS-CoV-2 nucleocapsid protein in nM (Table 2). Interestingly, ivermectin was predicted to be inactive as a NRL (BAS −2.94) whereas hydroxychloroquine was predicted to be moderately active as a NRL (BAS −0.12) and this was further validated with molecular docking analysis in which hydroxychloroquine exhibited 1000000x less affinity for nuclear receptor *i.e.* NRBD of SARS-CoV-2 nucleocapsid protein (K_d 1.25 mM) as compared to the *N. sativa* phytoconstituents which had their respective K_d in nM with respect to NRBD of SARS-CoV-2 nucleocapsid protein (Table 2). Though BAS as enzyme inhibitors were found to be >0.00 for all phytoconstituents, the highest score (0.66) was observed for citrostadienol and cycloartenol followed by tirucallol (0.64) and cycloeucalenol (0.61).

3.5. ADMET properties of phytocomponents

To check the pharmacokinetic feasibility of selected phytoconstituents from *N. sativa* as prospective drug candidates,

Table 4. Best docking poses of active components of *N. sativa* with N-terminal RNA binding domain (NRBD) of SARS-CoV-2 nucleocapsid protein (PDB ID: 6M3M) in comparison to standard drugs hydroxychloroquine and ivermectin. In AutoDock v4.2.6 analyses, ligand is represented as CPK model colored by- H = White, C = Grey, N = Blue, O = Red, S = Yellow, Pink = other elements. In AutoDock Vina, ligand is represented by 2-D line model, whereas in iGEMDOCK v2.1 analyses, ligand is represented by stick model. Green and blue dotted lines represent H- bond.

S. No.	Ligands	AutoDock v4.2.6	AutoDock Vina	iGEMDOCK v2.1
1.	24-methylene-cycloartanol	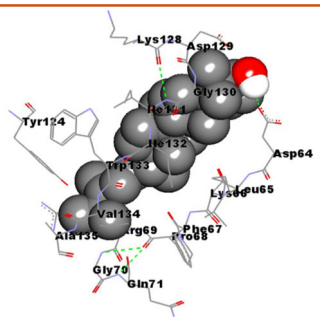	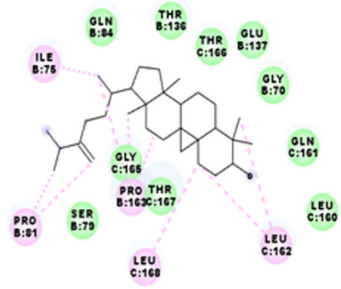	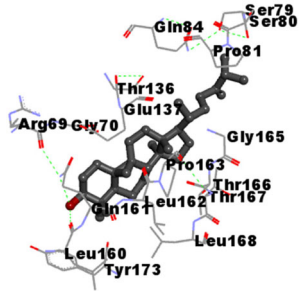
2.	Alpha-spinasterol	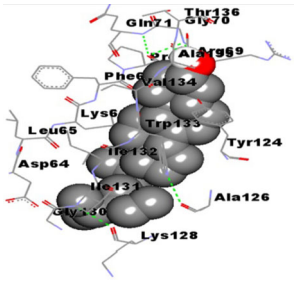	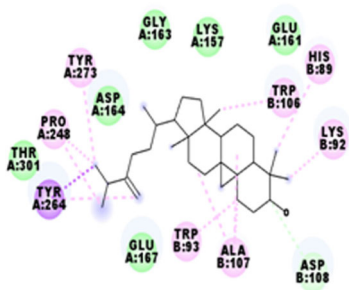	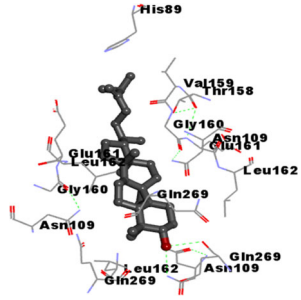
3.	Beta-sitosterol	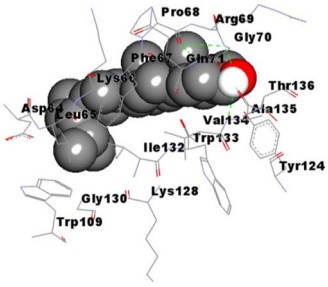	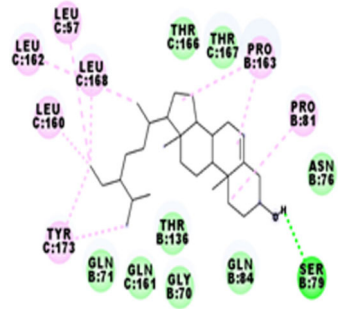	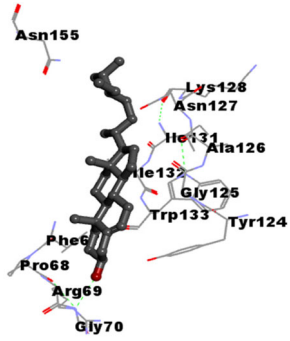
4.	Campesterol	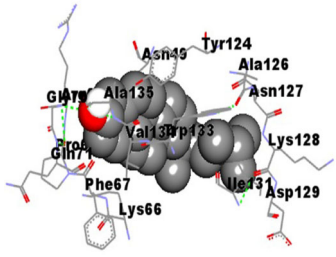	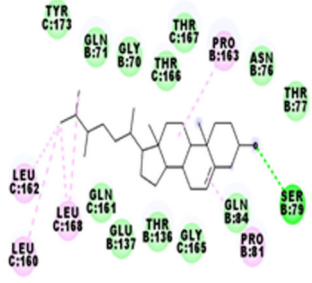	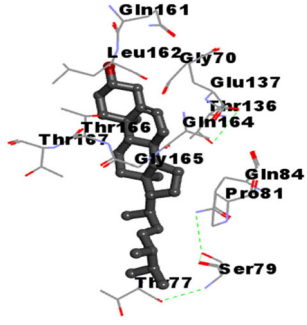
5.	Citrostadienol	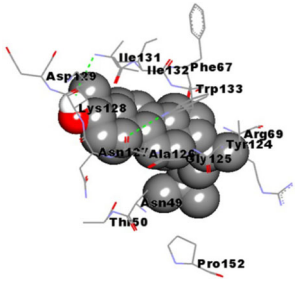	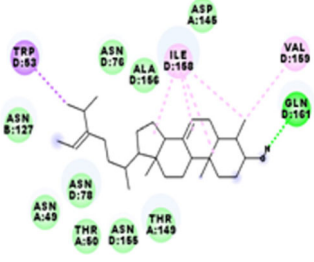	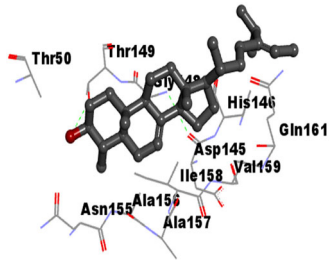

(*continued*)

Table 4. Continued.

S. No.	Ligands	AutoDock v4.2.6	AutoDock Vina	iGEMDOCK v2.1
6.	Taraxerol	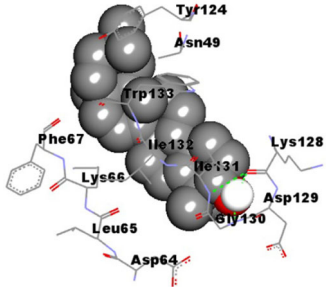	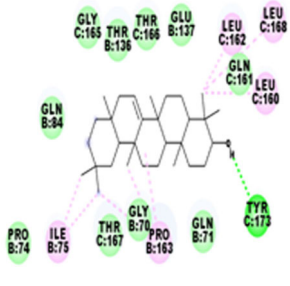	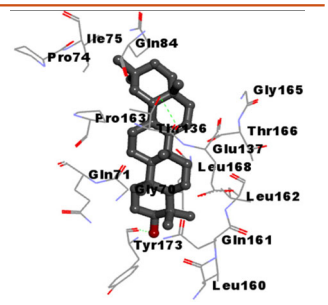
7.	Hydroxychloroquine	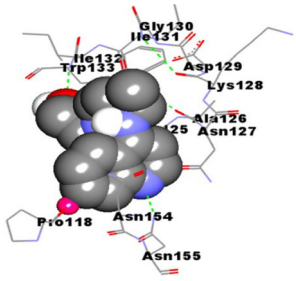	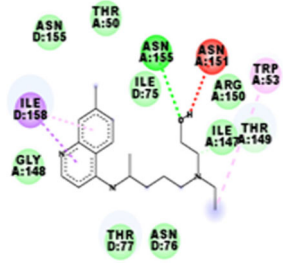	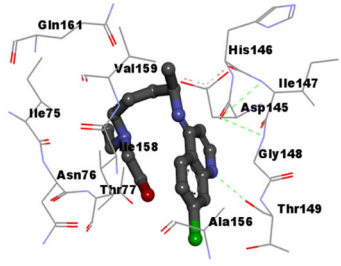
8.	Ivermectin	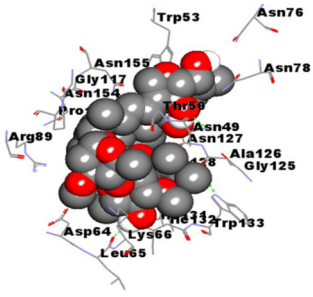	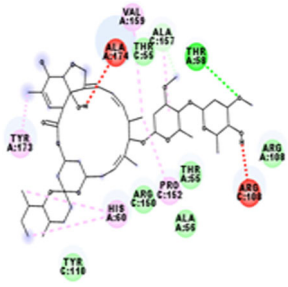	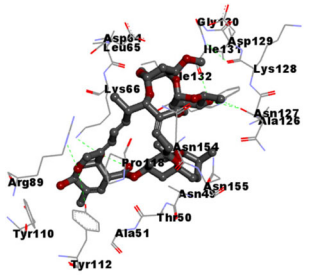

their ADMET properties *viz.* absorption, distribution, metabolism, excretion and toxicity were calculated using online SwissADME software (Table 9). Based on the calculated LogP value, all components were found to be lipid soluble (lipophilic) which indicates good absorption of all components across skin. Interestingly, neither of the phytocomponents displayed blood-brain barrier (BBB) permeability nor were predicted to act as permeability-glycoprotein (P-gp) substrates. P-gp is an ATP-dependent bioavailability protein pump that removes drugs from biological systems. The normal excretion of drugs back into the gut lumen by P-gp decreases the pharmacokinetics and efficacy of pharmaceutical drugs (which are said to be P-gp substrates). Since none of the *N. sativa* phytoconstituents were found to behave as P-gp substrates, they may be expected to persist in the cells and show their intracellular pharmacological (antiviral) effect, since the virus is also an intracellular pathogen. Interestingly, some cancer and virally infected cells have been found to express large amounts of P-gp. On the other hand, ivermectin was predicted to behave as a P-gp substrate, thereby raising the possibility of development of drug resistance in the near future against ivermectin by SARS-CoV-2 infected cells.

Cytochromes P450 (CYPs) are a superfamily of major metabolic enzymes involved in the biotransformation of xenobiotics. Drugs and other xenobiotics can act as both substrates and inhibitors of cytochromes P450 and they are involved in the metabolism of most medications. Drugs or compounds that inhibit the five classes of CYPs *viz.* CYP3A4, CYP1A2, CYP2C9, CYP2C19 and CYP2D6 would cause an increase in their plasma concentrations, thus contributing to improved bioavailability. In the present study, however, none of *N. sativa* phytocontistuents were found to act as inhibitors of the any of five classes of CYPs *versus* hydroxychloroquine which was found to act as inhibitor of CYP1A2 and CYP2D6 (Table 9). Skin permeability (Kp) is widely used to quantitatively describe the rate of chemical permeation through the outermost layer (epidermis) of the skin. Interestingly, all 10 phytocomponents showed negative Kp value which indicates less possibility of topical absorption of these phytoconstituents.

3.6. PCA of various phytoconstituents and standard drugs

PCA is a mathematical method to summarize multidimensional datasets into two or three principal components that can be visualized graphically with minimal loss of information. PCA was performed using OSIRIS Data Warrior v5.2.1 on three most variable properties *viz.* TPSA, %ABS and MW by applying linear correlation. The bar charts and 3D scatter plots of principal components to depict druglikeness of the phytoconstituents *versus* standard drugs were made in

Table 5. Best docking poses of active components of *N. sativa* with papain-like protease (PL_{-PRO}) of SARS-CoV-2 (PDB ID: 6W9C) *versus* standard drugs hydroxychloroquine and ivermectin.

S. No.	Ligands	AutoDock v4.2.6	AutoDock Vina	iGEMDOCK v2.1
1.	24-methylene-cycloartanol	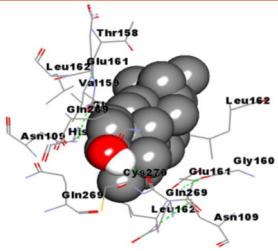	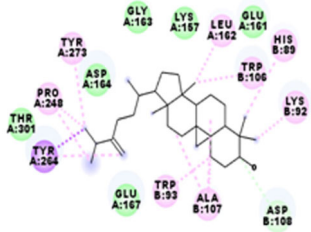	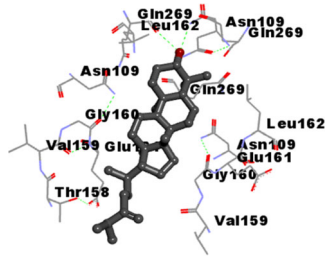
2.	Alpha-spinasterol	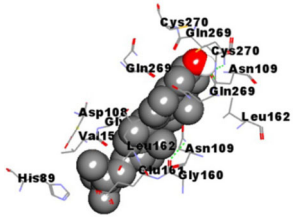	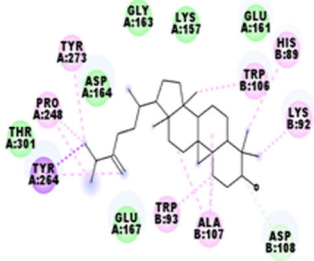	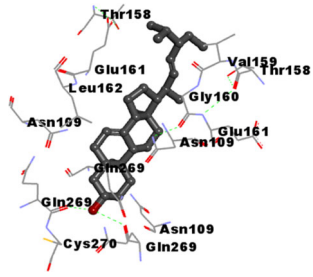
3.	Beta-amyrin	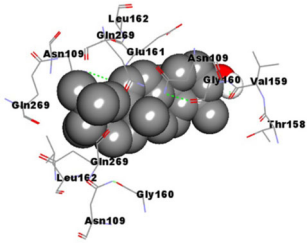	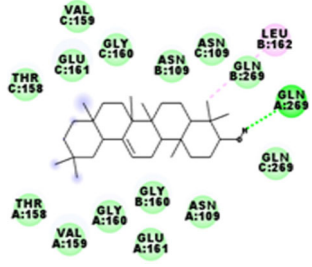	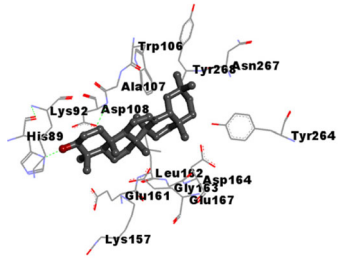
4.	Beta-sitosterol	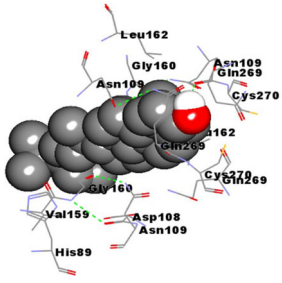	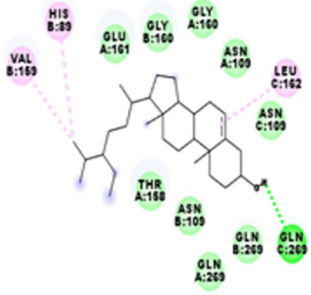	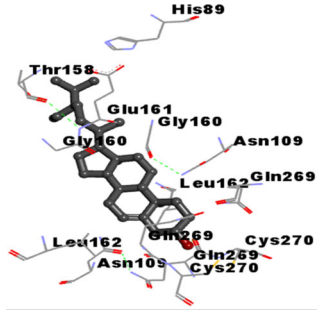
5.	Campesterol	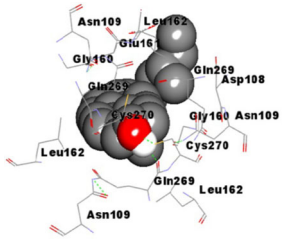	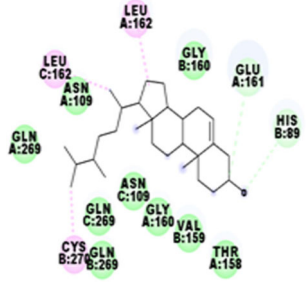	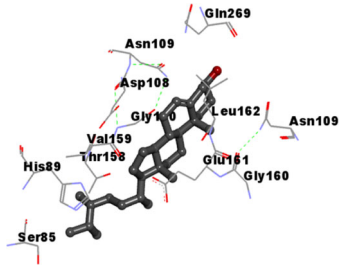
6.	Citrostadienol	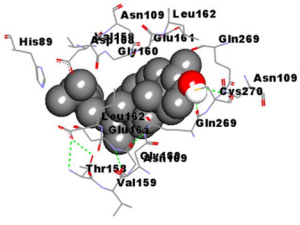	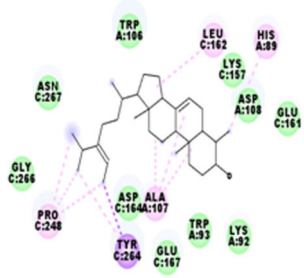	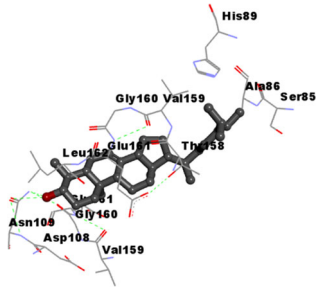

(*continued*)

Table 5. Continued.

S. No.	Ligands	AutoDock v4.2.6	AutoDock Vina	iGEMDOCK v2.1
7.	Cycloartenol	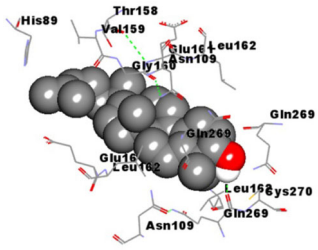	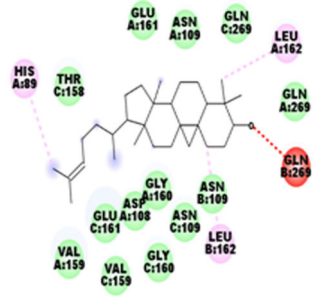	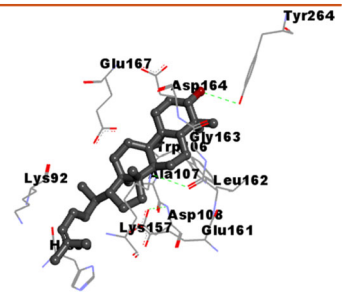
8.	Cycloeucalenol	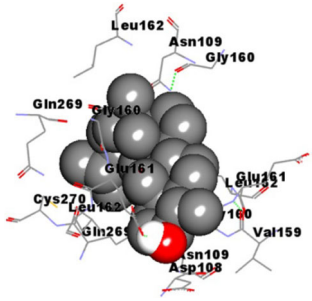	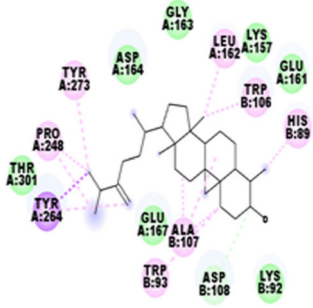	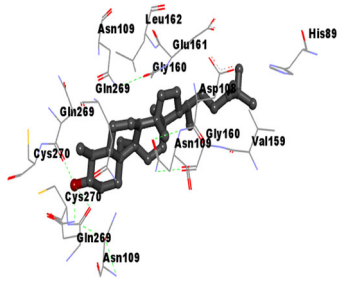
9.	Taraxerol	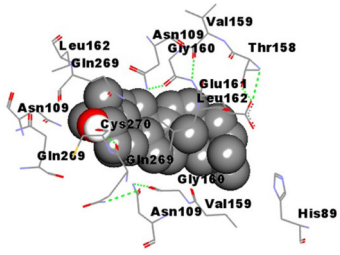	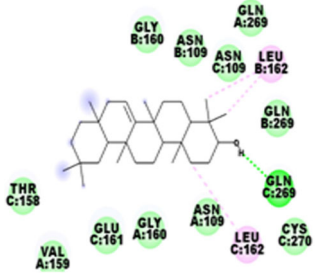	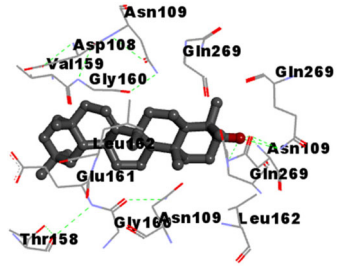
10.	Tirucallol	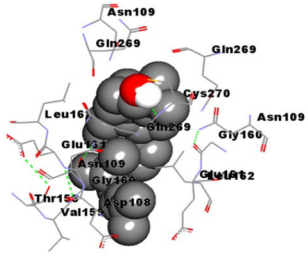	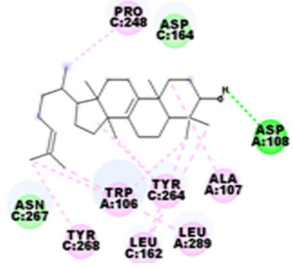	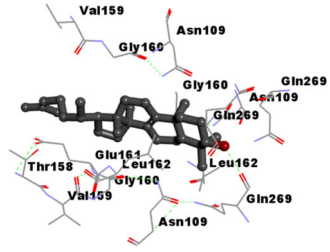
11.	Hydroxychloroquine	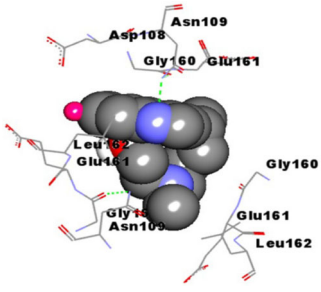	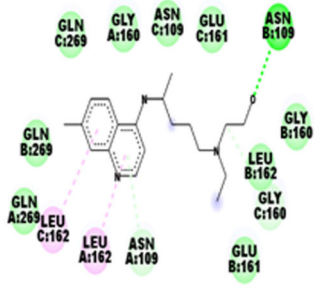	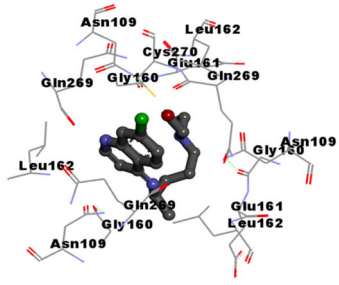
12.	Ivermectin	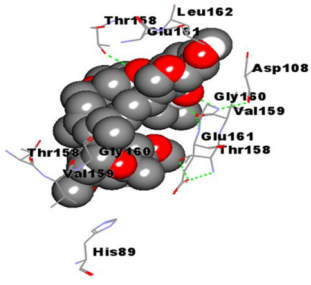	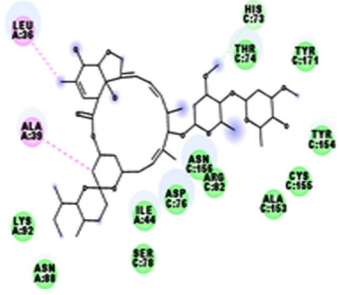	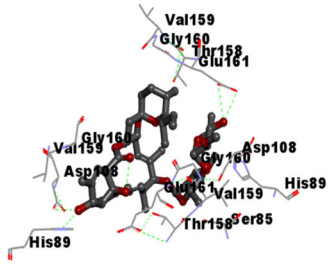

Table 6. PASS analysis of major active components of *N. sativa versus* standard antiviral drugs hydroxychloroquine and ivermectin.

Lipinski's rule of 5 (Physicochemical Properties)

S.No.	Phytoconstituents	% Absorption[a] (>50%)	Topological Polar Surface Area (Å)^2 (TPSA)[b] (<160 Å)	MW (<500)	c logP[c] (<5)	Heavy atom count (n atoms)	Hydrogen Bond Donors (nOHNH) (≤5)	Hydrogen Bond Acceptors (nON) (≤10)	Number of Rotatable bonds (≤10)	Lipinski's violation
1.	24-methylene-Cycloartanol	102.02	20.23	440.76	8.03	32	1	1	5	1
2.	Alpha-spinasterol	102.02	20.23	412.70	7.87	30	1	1	5	1
3.	Beta-amyrin	102.02	20.23	426.73	8.02	31	1	1	0	1
4.	Beta-sitosterol	102.02	20.23	414.72	8.62	30	1	1	6	1
5.	Campesterol	102.02	20.23	400.69	8.30	29	1	1	5	1
6.	Citrostadienol	102.02	20.23	426.73	8.15	31	1	1	5	1
7.	Cycloartenol	102.02	20.23	426.73	8.21	31	1	1	4	1
8.	Cycloeucalenol	102.02	20.23	426.73	7.62	31	1	1	5	1
9.	Taraxerol	102.02	20.23	426.73	8.02	31	1	1	0	1
10.	Tirucallol	102.02	20.23	426.73	8.48	31	1	1	4	1
11.	Hydroxychloroquine	92.16	48.38	335.88	4.00	23	2	4	9	0
12.	Ivermectin	50.31	170.09	875.11	4.58	62	3	14	8	3

Note:.
[a]Percentage Absorption was calculated as: % Absorption =109- [0.345xTopological Polar Surface Area].
[b]Topological polar surface area (defined as a sum of surfaces of polar atoms in a molecule).
[c]Logarithm of compound partition coefficient between n-octanol and water.

OSIRIS Data Warrior v5.2.1 and Discovery Studio Visualizer 2017 R2, respectively (Figure 1A and B). As depicted earlier, MWs of all the phytocomponents of *N. sativa* were <500 and, therefore, it can be expected that all the phytocomponents would be easy to transport, diffusible and readily absorbed. However, the MW of standard drug ivermectin was found to be >500 thereby showing serious limitations in its transportation, diffusion and absorption. As is evident from Figure 1A and B, all the phytoconstituents of *N. sativa* appear close to each other in scatter and 3D plot, which means that the *N. sativa* phytoconstituents have more or less similar properties in the context of TPSA, %ABS and MW *versus* standard reference drugs. Table 10 represents the Bravais-Pearson (linear correlation) coefficient of *N. sativa* phytoconstituents *versus* standard drugs. This type of matrix correlation represents 'druglike' property of the phytoconstituents.

3.7. Structure activity relationship (SAR)

N. sativa contains various phytochemicals belonging to the class of terpenoids and flavonoids; the major ones have been listed in Table S1. Out of twenty five phytocomponents, ten components showed strong binding affinity with targeted proteins of SARS-CoV-2. Based on the structural relationship, all ten components can be divided into three parent configurations as shown in Figure 2. All compounds displayed a similar backbone structure with four rings arranged in a specific molecular configuration. This steroidal backbone is derived from sterol cycloartenol in plants cells. Cycloartenol is an important triterpenoid of the class sterol, which is the starting point for the synthesis of almost all plant steroids. Further, cycloartenol is derived from the cyclization of the triterpene squalene having molecular formula $C_{30}H_{48}$. In this study, the differential binding kinetics obtained for alpha-spinasterol (MF: $C_{29}H_{48}O$; MW: 412.7), beta-sitosterol (MF: $C_{29}H_{50}O$; MW: 414.7) and campesterol (MF: $C_{28}H_{48}O$; MW: 400.7) with N-terminal RNA binding domain (NRBD) of SARS-CoV-2 nucleocapsid protein (PDB ID: 6M3M) may be attributed to the variation in the number of alkyl groups (Figure 2A) in their backbone structures which might affect hydrogen bonding within the binding site of the targeted viral protein(s). Similarly, the variations in binding kinetics obtained for campesterol, cycloeucalenol (MF: $C_{30}H_{50}O$; MW: 426.7) and alpha-spinasterol with papain-like protease ($PL\text{-}_{PRO}$; PDB ID: 6W9C) of SARS-CoV-2 may also be attributed to the variation in the number of alkyl side groups in their backbone structures which might affect hydrogen bonding within the binding pockets of the amino acid residues in target protein(s). In addition, another reason for differential SARs among various types of *N. sativa* phytoconstituents might be attributed to structural differences in alkene and cycloalkane groups along with spatial and stereochemical configurations of alkane groups, which cause the structural rearrangement as shown in Figure 2. These structural variations might be responsible for a better complementary fit of the phytocomponents in the binding pocket of the viral protein(s).

Table 7. Druglikeness and toxicity calculations of *N. sativa* phytoconstituents *versus* standard drugs hydroxychloroquine and ivermectin.

		Druglikeness and Toxicity parameters				
S. No.	Compounds Name	Druglikeness	Mutant	Tumurogenic	Reproductive effective	Irritant
1.	24-Methylene-Cycloartanol	−9.2281	N	N	N	N
2.	Alpha-Spinasterol	1.2217	N	L	N	N
3.	Beta-Amyrin	−2.4858	N	N	N	N
4.	Beta-Sitosterol	−4.475	N	N	N	N
5.	Campesterol	−8.1908	N	N	N	N
6.	Citrostadienol	−5.602	N	N	N	H
7.	Cycloartenol	−4.1078	N	N	N	H
8.	Cycloeucalenol	−7.633	N	N	N	N
9.	Taraxerol	−2.422	N	N	N	N
10.	Tirucallol	−4.1331	N	N	H	H
11.	Hydroxychloroquine	5.7266	H	N	N	N
12.	Ivermectin	5.2314	N	N	N	N

N- No toxicity.
L- Low toxicity.
H- High toxicity.

Table 8. Bioactivity scores of *N. sativa* phytoconstituents *versus* standard drugs hydroxychloroquine and ivermectin.

		Parameters of bioactivity score (BAS)					
S. No.	Phytocomponents	GPCR Ligand	Ion Channel Modulator	Kinase Inhibitor	Nuclear Receptor Ligand	Protease Inhibitor	Enzyme Inhibitor
1.	24-Methylene-Cycloartanol	0.14	0.11	−0.37	0.90	0.06	0.60
2.	Alpha-Spinasterol	0.18	0.05	−0.30	0.68	0.06	0.53
3.	Beta-Amyrin	0.22	−0.05	−0.31	0.67	0.11	0.56
4.	Beta-Sitosterol	0.14	0.04	−0.50	0.73	0.07	0.51
5.	Campesterol	0.11	0.01	−0.48	0.71	0.01	0.50
6.	Citrostadienol	0.15	0.15	−0.34	0.89	0.13	0.66
7.	Cycloartenol	0.21	0.10	−0.40	0.86	0.14	0.66
8.	Cycloeucalenol	0.14	0.14	−0.37	0.92	0.10	0.61
9.	Taraxerol	0.21	0.02	−0.20	0.54	0.00	0.49
10.	Tirucallol	0.18	−0.05	−0.39	0.82	0.06	0.64
11.	Hydroxychloroquine	0.35	0.30	0.44	−0.12	0.12	0.15
12.	Ivermectin	−2.49	−2.86	−3.23	−2.94	−1.89	−2.53

Table 9. ADMET properties calculated for *N. sativa* phytoconstituents *versus* standard drugs hydroxychloroquine and ivermectin.

S.No.	Phytocomponents	Lipophilicity (Consensus Log $P_{o/w}$)	BBB permeant	P-gp substrate	CYP1A2 inhibitor	CYP2C19 inhibitor	CYP2C9 inhibitor	CYP2D6 inhibitor	CYP3A4 inhibitor	Log Kp (skin permeation)
1.	24-methylene-cycloartanol	7.79	No	No	No	No	No	No	No	−1.67 cm/s
2.	Alpha-spinasterol (spinasterol)	6.88	No	No	No	No	No	No	No	−2.92 cm/s
3.	Beta-amyrin	7.18	No	No	No	No	No	No	No	−2.41 cm/s
4.	Beta-sitosterol	7.19	No	No	No	No	No	No	No	−2.20 cm/s
5.	Campesterol	6.90	No	No	No	No	No	No	No	−2.50 cm/s
6.	Citrostadienol (alpha1-sitosterol)	7.26	No	No	No	No	No	No	No	−2.49 cm/s
7.	Cycloartenol	7.51	No	No	No	No	No	No	No	−1.96 cm/s
8.	Cycloeucalenol	7.45	No	No	No	No	No	No	No	−1.87 cm/s
9.	Taraxerol	7.22	No	No	No	No	No	No	No	−2.30 cm/s
10.	Tirucallol	7.42	No	No	No	No	No	No	No	−2.58 cm/s
11.	Hydroxychloroquine	3.37	Yes	No	Yes	No	No	Yes	No	−5.81 cm/s
12.	Ivermectin	4.35	No	Yes	No	No	No	No	No	−7.14 cm/s

3.8. Molecular dynamics (MD) simulation

MD simulation provides information about structural and conformational fluctuations over time and thermodynamics of biological molecules and their complexes. Figures 3 and 4 and Supplementary Figures S1, S2, S3 & S4 describe the MD simulation analysis of cycloeucalenol with PL-$_{PRO}$ (PDB ID: 6W9C) and alpha-spinasterol with NRBD of nucleocapsid protein (PDB ID: 6M3M) of SARS-CoV-2, respectively. The stability of both protein-ligand complexes was assessed through the trajectory analysis obtained through RMSD, RMSF, radius of gyration (Rg), and fraction of native contacts (Qx) analysis over a time frame of 4000ps (4 ns).

RMSD is the measurement of the average distance between the atoms of the overlaid structures. Often, equalized RMSD plots indicate that the system is in equilibrium. In the present study, MD simulation analyses showed a satisfactory stability profile at 300 K temperature.Cycloeucalenol-PL-$_{PRO}$ complex displayed very low deviation in RMSD from 1-3.6 Å throughout the 4 ns simulation (Figure 3). Likewise alpha-spinasterol with NRBD of SARSCoV-2 complex also exhibited less deviation in RMSD from 1-2.6 Å throughout the 4 ns time scale (Figure 4). Results from RMSD analysis of both complexes suggested that the deviation in the RMSDs was low; which indicated good stability and compactness of both protein-ligand complexes. The radius of gyration (Rg) of

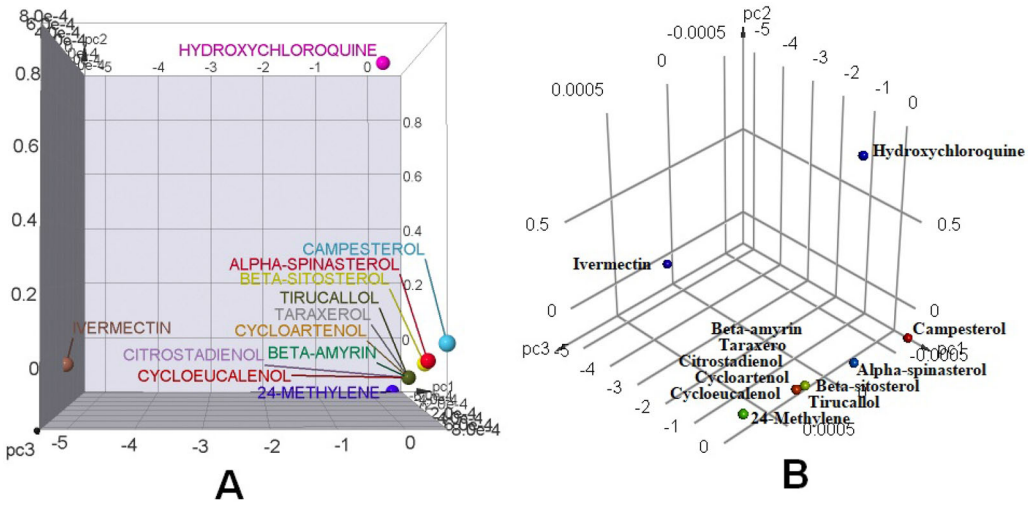

Figure 1. PCA of leadlikeness of *N. sativa* phytoconstituents *versus* antiviral standard drugs hydroxychloroquine and ivermectin (A) Scatter plot (B) 3 D point plot.

Table 10. Bravais-Pearson (linear correlation) coefficient of *N. sativa* phytoconstituents *versus* standard drugs hydroxychloroquine and ivermectin.

Properties		1	2	3	4	5	6	7	8	9	10	11	12
% Ab	1		−1	−0.927	0.739	−0.908	−0.958	−1	−0.496	−0.597	0.992	−0.126	2.74E-04
TPSA	2	−1		0.928	−0.737	0.909	0.957	1	0.494	0.599	−0.992	0.123	2.76E-04
MW	3	−0.927	0.928		−0.449	1	0.784	0.912	0.273	0.848	−0.967	−0.255	−2.04E-06
logP	4	0.739	−0.737	−0.449		−0.407	−0.894	−0.764	−0.646	0.0812	0.654	−0.717	0.175
natoms	5	−0.908	0.909	1	−0.407		0.752	0.891	0.241	0.873	−0.953	−0.302	0.00361
nOHNH	6	−0.958	0.957	0.784	−0.894	0.752		0.969	0.609	0.343	−0.915	0.399	−0.0561
nON	7	−1	1	0.912	−0.764	0.891	0.969		0.514	0.565	−0.986	0.164	−0.00802
Rb	8	−0.496	0.494	0.273	−0.646	0.241	0.609	0.514		0.0808	−0.429	0.556	0.0925
LV	9	−0.597	0.599	0.848	0.0812	0.873	0.343	0.565	0.0808		−0.691	−0.705	0.156
pc1	10	0.992	−0.992	−0.967	0.654	−0.953	−0.915	−0.986	−0.429	−0.691		−1.23E-10	1.14E-09
pc2	11	−0.126	0.123	−0.255	−0.717	−0.302	0.399	0.164	0.556	−0.705	−1.23E-10		3.36E-09
pc3	12	2.74E-04	2.76E-04	−2.04E-06	0.175	0.00361	0.0561	−0.00802	0.0925	0.156	1.14E-09	3.36E-09	

the body on the axis of rotation is considered to be the radial distance of a point from the axis of rotation. It is among the most significant indicators that are commonly used in the prediction of the structural activity and folding behavior of a macromolecule. Once the folding state of the protein is changed, the gyration radius would be affected. Rg of cycloeucalenol-PL-$_{PRO}$ of SARS-CoV-2 was found to be around 30.8, and it was 31.0 for alpha-spinasterol-NRBD of SARS-CoV-2 complex throughout the 4 ns simulations which suggested that there was little change in the compactness of the complex structure during the simulation indicating strong structural stability of both ligand-protein complexes (Figures 3E and 4E). Further, to calculate the average fluctuation of all residues during simulations, RMSFs of both target proteins were plotted using ligand-protein complexes. RMSF values are used to determine the atomic positional fluctuation of each residue *via* calculation based on the C-alpha (Cα) atom of them. The comparative analysis of RMSF trajectories revealed that all the residues in the complex model of cycloeucalenol-PL-$_{PRO}$ of SARS-CoV-2 fluctuated between 4-8 Å (Figure 3H), while in case of alpha-spinasterol with NRBD of SARS-CoV-2, RMSF value was found to fluctuate between 5-15 Å (Figure 4H). In the folding process, certain cases of non-native interactions are considered to be irrelevant and there are certain simulations as well as folding models which support that only native contacts are energetically favorable. Therefore, fraction of native contacts Q (x) helps in capturing the transition states remarkably well for all proteins along with a folding free energy barrier. In the present study, the Qx value was found to be larger than 95% in both complexes. This result indicates the relative flexibility and increased stability of both complexes throughout the simulation period (Figures 3F and 4F). B-factor, also termed as the temperature factor, which is similar to RMSF and is used to describe the attenuation of x-ray scattering resulting due to thermal motion. The result of B-factors of both complexes revealed that cycloeucalenol-PL-$_{PRO}$ of SARS-CoV-2 fluctuated around 2000 while alpha-spinasterol-NRBD of SARS-CoV-2 fluctuated around 5000 of B-factors, which indicated thermal stability of the complex.

PCA is used to detect nature of conformational differences, while magnitude of pairwise cross-correlation coefficients indicates system's atomic variations associated with each other. As shown in Figure S1 and S3, the correlated residues are blue colored whereas, non-correlated residues are in red. The light pink and light blue lines represent pairwise residues with higher correlated coefficient (>0.8) and with higher non-correlated coefficient (<-0.4). The schematic representation of secondary structures are present on the top and right margins of dynamic residue cross-correlation map appearing in black helices , grey strands and white loops . MM/PB(GB)SA result analysis mainly comprises electrostatic energy (ELE), van der Waals contribution (VDW), total gas phase energy (GAS), non-polar and polar

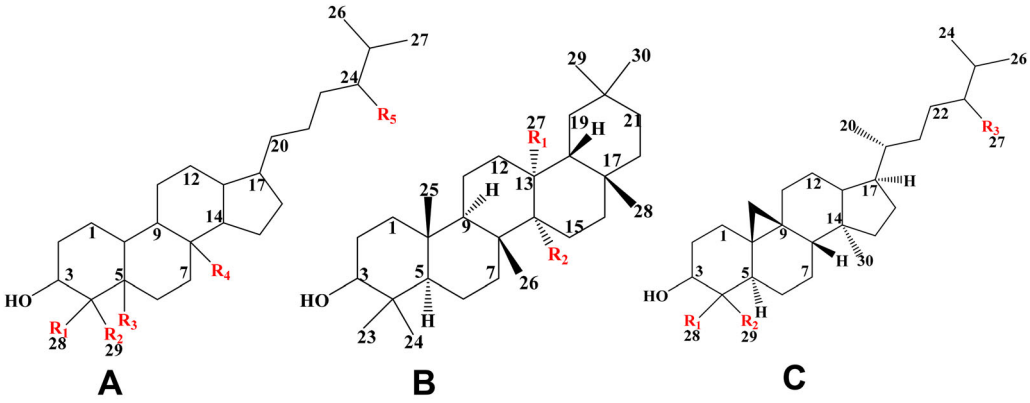

(b) R_1 =H, R_5 = C_2H_5
(d) R_4= H, R_5= C_2H_5
(e) R_4=H, R_5= CH_3
(f) R_1 =H, R_2= CH_3, R_5= CH-$(CH_3)_2$
(j) R_1 =H, R_2, R_3 = CH_3

(c) R_2= H
(i) R_1= H

(a) R_1 and R_2= CH_3, R_3 =CH_2
(g) R_1 and R_2= CH_3, R_3 = H
(h) R_1= CH_3, R_3 = CH_2

Figure 2. Structural differences in 10 phytocomponents of *N. sativa* divided into three groups: Group (A) (b) alpha-spinasterol, (d) beta-sitosterol, (e) campesterol, (f) citrostadienol and (j) tirucallol; Group (B) (c) beta-amyrin and (i) taraxerol; Group (C) (a) 24-methylene-cycloartanol, (g) cycloartenol and (h) cycloeucalenol.

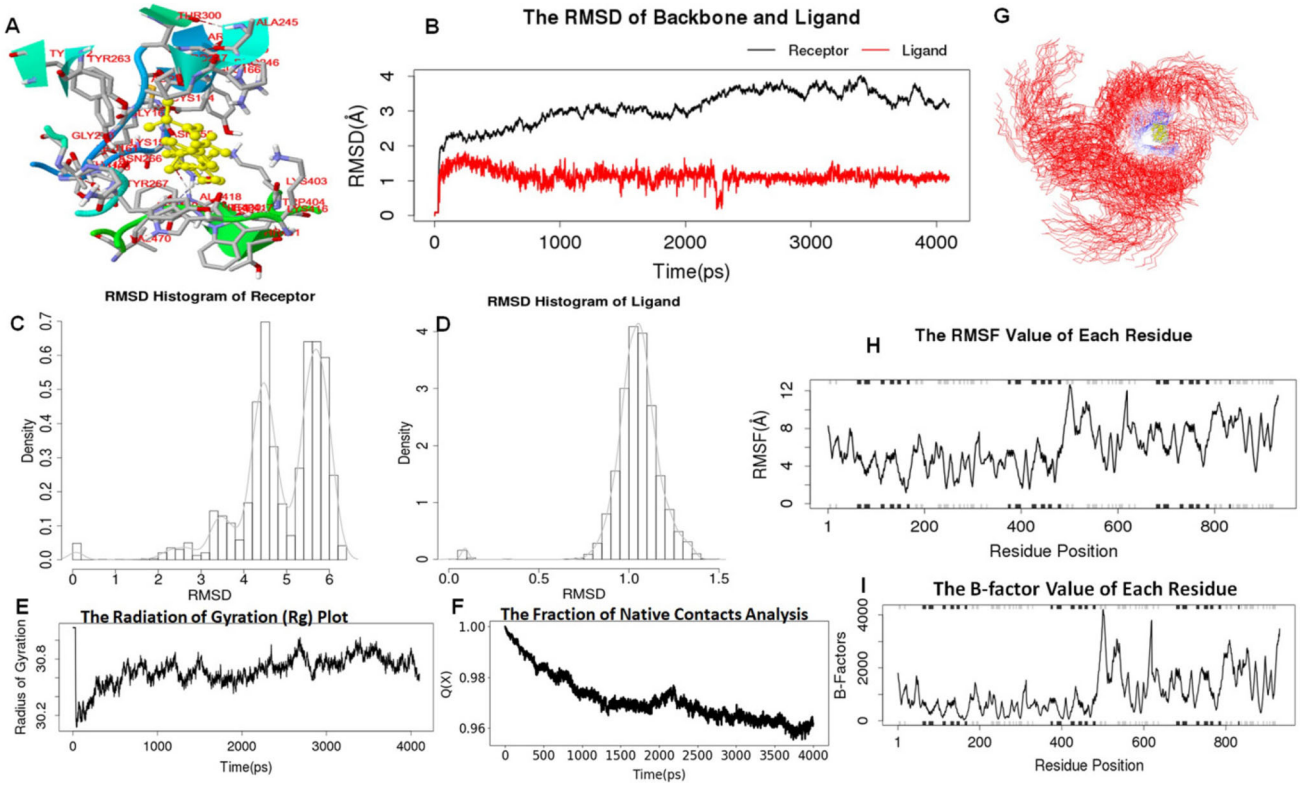

Figure 3. RMSD values of SARS-CoV-2 PL-$_{PRO}$ (PDB ID: 6W9C) complexed with cycloeucalenol were analyzed as a function of time at 300 K. Values were calculated with the use of Cα atoms. (A) Ligand-protein conformation (B) RMDS of receptor and ligand (C) RMSD histogram of receptor (D) RMSD histogram of ligand (E) Radiation of Gyration- Rg value (F) Fraction of native contacts analysis of SARS-CoV-2 PL-$_{PRO}$ (PDB ID: 6W9C) with cycloeucalenol, over a time frame of 4000ps (4 ns) (G) B-factor value (changing from blue to red with increase in value) (H) RMSF value of each residue and (I) B-factor analysis of defined complex.

contributions to solvation (PBSOL/GBSOL). The finally recorded binding free energy (deltaPB/deltaGB) is calculated from PBTOT/GBTOT and entropy (TS) as shown in Figures S2 A and S4 A. Further, hydrogen bond analysis includes the hydrogen bond acceptor and donor atoms, average distance (AvgDist), angle (AvgAng), and proportion (Frac) as shown in Figures S2 B and S4 B. Moreover, the results of decompose comprises of electrostatic energy which is calculated by the MM force field (TELE), van der Waals contribution from MM (TVDW), sum of non-polar and polar contributions to solvation (TGBSOL), total gas phase energy (TGAS) and final estimation of binding free energy from TGBTOT. Depending on the TGBTOT energy, the residues with contribution are ranked into top 10 decompose calculations which are arranged from top to bottom in heatmap (Figures S2 C and S4 C).

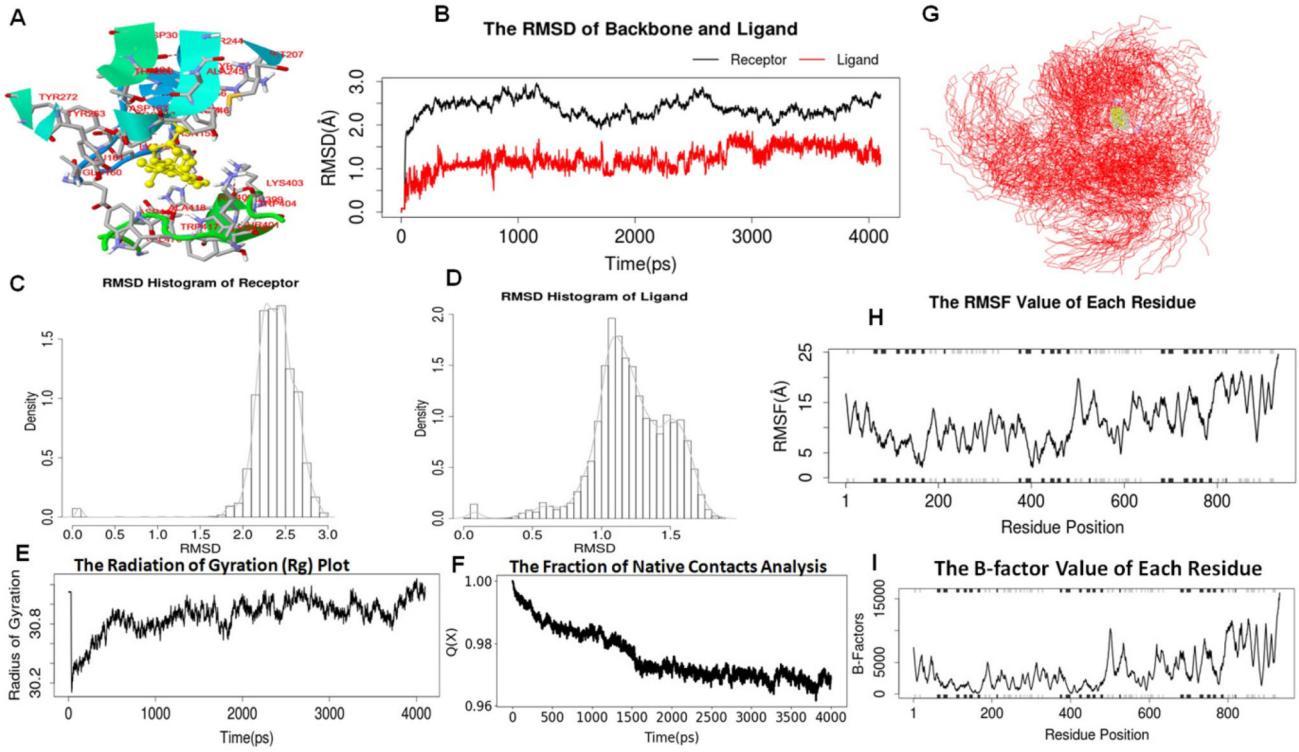

Figure 4. RMSD values of NRBD of SARS-CoV-2 nucleocapsid protein (PDB ID: 6M3M) comlexed with alpha-spinasterol were analyzed as a function of time at 300 K. Values were calculated with the use of Cα atoms. (A) Ligand-protein conformation (B) RMDS of receptor and ligand (C) RMSD histogram of receptor (D) RMSD histogram of ligand (E) Radiation of Gyration- Rg value (F) Fraction of Native Contacts Analysis of SARS-CoV-2 NRBD of nucleocapsid protein (PDB ID: 6M3M) with alpha-spinasterol, over a time frame of 4000ps (4 ns) (G) B-factor value (changing from blue to red with increase in value) (H) RMSF value of each residue and (I) B-factor analysis of defined complex.

4. Discussion

Coronavirus disease (COVID-19) is an infectious pandemic that emerged from China and caused deadly outbreaks in USA, UK, Europe and middle east and far east countries including India and Pakistan (Hassan et al., 2020). The ongoing SARS-CoV-2 pandemic has spawned extensive research in identifying therapeutic targets and development of therapeutic drugs without any side effects. Although various antiviral and antimalarial drugs *viz.* umifenovir, remdesivir, lopinavir, favipiravir, ritonavir, ivermectin, hydroxychloroquine, chloroquine and azithromycin are being used currently to treat COVID-19 (Patil et al., 2020), however, these drugs cause various critical side effects including nervousness, poor concentration, nausea, vomiting, and diarrhoea. In addition, various risk factors such as the elderly and people suffering from pre-existing medical conditions like heart disease, respiratory disease or diabetes have a higher risk of dying from COVID-19 (https://www.drugs.com/condition/covid-19.html). Therefore, finding board-spectrum inhibitors that may reduce the effects of human corona virus infection along with reducing side effects remains a challenging research focus. Complementary and alternative medicine entails a variety of herbal plants, which may have potential for alternative drug development against COVID-19. The plant-derived products also act as immunomodulators without undesirable side effects. Further, virtual screening methods of ligand-protein interactions using computer-assisted drug design tools such as molecular docking and MD simulation analysis are the preliminary steps that lead to further development of potential therapeutic compounds in drug development process.

In the present study, an attempt has been made to explore the antiviral potential of selected phytochemicals of *N. sativa* belonging to the class of terpenoids and flavonoids against five target proteins of SARS-CoV-2 especially NRBD of nucleocapsid protein and PL-$_{PRO}$ using molecular and chemoinformatic tools and *in silico* approaches. For this study, twenty five phytocomponents were selected from black cumin seeds and oil based on their structure-activity relationships and prospective targeted metabolic pathways using Dr. Duke's Phytochemical and Ethnobotanical Database. Based on the best binding energies and K_d of ligand-protein interactions with AutoDock v4.2.6, out of twenty five phytocomponents, ten active components with their targeted proteins *viz.* NRBD of nucleocapsid protein and PL-$_{PRO}$ of SARS-CoV-2 were selected for further validation using two other molecular docking tools *viz.* AutoDock Vina and iGEMDOCK v2.1. Interestingly, these two proteins play key roles in viral replication and assembly in host cells and, as such, can be used as therapeutic targets for antiviral drug discovery. Both PL-$_{PRO}$ and 3CL-$_{PRO}$ are involved in the processing of viral polyproteins (PPs) in a coordinated manner which is essential for viral replication. However, PL-$_{PRO}$ has the additional function of stripping ubiquitin and ubiquitin-like protein ISG15 (Interferon-stimulated gene 15) from host-cell proteins to help CoV to escape the host innate immune responses (Báez-Santos et al., 2015). Therefore, targeting PL-$_{PRO}$ with antiviral drugs might have an advantage in not only

inhibiting viral replication but also inhibiting the dysregulation of signaling cascades in infected cells that might lead to cell death of surrounding uninfected cells. Nucleocapsid protein consists of three distinct but highly conserved parts: N terminal domain (NTD), Ser/Arg (SR)-rich central linker (CL) and C terminal domain (CTD). The most important function of NTD of nucleocapsid protein is RNA binding, while CTD acts as a dimerization domain, and, thus, also helps in packaging of SARS-CoV viral RNA into a long helical nucleocapsid structure or ribonucleoprotein (RNP) complex, which plays a fundamental role during viral self-assembly (Chang et al., 2014).

Results of molecular docking analysis using AutoDock v4.2.6 have shown that alpha-spinasterol (BE = −9.54 kcal/mol, K_d = 101.42 nM) has the best binding affinities with NRBD of SARS-CoV-2 followed by beta-sitosterol (BE = −8.69 kcal/mol, K_d = 426.43 nM) and campesterol (BE = −8.57 kcal/mol, K_d = 522.64 nM). However, taraxerol (BE = −12.1 kcal/mol, K_d = nM) and 24-methylene-cycloartanol (TE = −96.16 kcal/mol) exhibited best binding affinity as analyzed by AutoDock Vina and iGEMDOCK v2.1, respectively. In case of binding interaction with PL-$_{PRO}$ of SARS-CoV-2, campesterol (BE = −9.7 kcal/mol, K_d = 76.87 nM) has shown the best binding affinities followed by cycloeucalenol (BE = −9.65 kcal/mol, K_d = 84.23 nM) and alpha-spinasterol (BE = −9.41 kcal/mol, K_d = 126.53 nM) as analyzed by AutoDock v4.2.6. On the other hand, taraxerol (BE = −10.0 kcal/mol) and cycloeucalenol (TE = −102.07 kcal/mol) exhibited best binding affinity with PL-$_{PRO}$ as analyzed by AutoDock Vina and iGEMDOCK v2.1, respectively. Interestingly, this study is in agreement with a previously published report where steroidal glycoalkaloids from *Solanum nigrum* have shown similar kind of variation in binding energy with their selected protein targets (Ahmad, 2019). These results suggest that minor variations in binding affinity of the phytocomponents is because of the differences in the generation of grid boxes and determination of binding pockets on the target proteins by these softwares on account of slight differences in selection criteria. This has led to a difference in interacting amino acid residues in the binding pockets of NRBD of nucleocapsid protein and PL-$_{PRO}$ of SARS-CoV-2 as is evident from Tables 2 and 3. On the basis of their binding energies and K_d values, campesterol, alpha-spinasterol and cycloeucalenol have been found to be the most effective phytocomponents in *N. sativa* against SARS-CoV-2. In this study, hydroxychloroquine and ivermectin were selected as standard reference drugs since they have shown antiviral effects against several distinct negative-sense single-strand RNA viruses, including SARS-CoV-2 (Heidary & Gharebaghi, 2020; Rebeaud & Zores, 2020).

MD simulations are valuable methods for understanding the dynamic behavior of biological macromolecules at different timescales. RMSD is always non-negative, and a value of 0, although never achieved in practice, indicates a perfect fit to the data. In general, lower the RMSD, better the model is in comparison to the target structure. When a dynamic system fluctuates about a well-defined average position, the RMSD from the average over a time frame can be referred to as the RMSF. Interestingly, in the present study, the high affinity complexes *viz.* alpha-spinasterol with NRBD of nucleocapsid protein and cycloeucalenol with PL-$_{PRO}$ of SARS-CoV-2 complex displayed a very low deviation of 0.5-2.0 Å and 0.1-2.6 Å, respectively, throughout the 4 ns time scale (Figures 3 and 4), which indicated a good stability of both protein-ligand complexes. Moreover, results from RMSF, Rg, and Qx analyses over a time frame of 4 ns along with B-factors suggested the thermodynamic stability of both complexes.

In the drug discovery context, all ten active phytocomponents were tested for their druglikeness using Lipinski's rule of five. Lipinski's rule of five predicts that strong absorption/permeation is more likely when the MW <500, the calculated LogP (cLog P) ≤5.0, there are ≤5 H-bond donors and ≤10 H-bond acceptors. Generally, an orally active compound should have no more than one Lipinski's violation otherwise its bioavailability is compromised (Lipinski, 2004). Interestingly, all ten phytoconstituents from *N. sativa* exhibited only one Lipinski's violation. Therefore, it can be postulated that all ten phytocomponents have the potential to be evaluated further from a drug development perspective. Further, toxicity potential assessment is essential for avoiding unsuitable substances for further drug screening in order to initiate *in vitro* and *in vivo* evaluation (Parasuraman, 2011). The phytocomponents were screened for their mutagenic, tumorigenic, irritant and reproductive toxicity risk assessment. Most of the phytocomponents such as 24-methylene-cycloartanol, alpha-spinasterol, beta-amyrin, beta-sitosterol, campesterol, cycloeucalenol and taraxerol were found to be safe with no predicted toxicity. Further, all phytocomponents displayed a lipophilic nature which indicated good absorption and transport kinetics through the gut. Principal component analysis revealed that all phytoconstituents of *N. sativa* fell close to each other and also near to standard drug hydroxychloroquine in scatter and 3D plots representing their drug like properties.

In conclusion, NRBD of nucleocapsid protein and PL-$_{PRO}$ of SARS-CoV-2 have been revealed as important drug targets for *N. sativa* phytoconstituents . As revealed in section 3.4 and discussion section, the selected phytoconstituents of *N. sativa* were found to behave as protease inhibitors going by their BAS scores of >0.00, thus, lending credibility to the selection of viral PL-$_{PRO}$ as a drug target in the present study. The most effective phytocomponents *viz.* campesterol, cycloeucalenol, alpha-spinasterol and beta-sitosterol exhibited high affinities against NRBD and PL-$_{PRO}$ of SARS-CoV-2. Owing to their bioavilability, druglikeness and almost zero toxic and mutagenic effects, these phytoconstituents can be explored further *in vitro* and *in vivo* as potential antiviral agents for the treatment of COVID-19 .

Acknowledgements

The authors gratefully acknowledge Dr. Meraj Ahmad, Professor, Dept. of Sociology, University of Lucknow, Lucknow, India, for being the inspiration and motivation behind the present work in view of his exceptional work and contribution in the area of social sciences, humanities and public health. Maqusood Ahamed is also grateful to the Researchers

Supporting Project number (RSP- 2020/129), King Saud University, Riyadh, Saudi Arabia.

Disclosure statement

The authors declare that they have no competing interests.

ORCID

Sahabjada Siddiqui http://orcid.org/0000-0003-0982-1465
Shivbrat Upadhyay http://orcid.org/0000-0002-9938-0810
Rumana Ahmad http://orcid.org/0000-0002-7535-4976
Anamika Gupta http://orcid.org/0000-0003-2334-7958
Aditi Srivastava http://orcid.org/0000-0003-3141-7311
Anchal Trivedi http://orcid.org/0000-0002-4804-9925
Ishrat Husain http://orcid.org/0000-0001-6963-7171
Bilal Ahmad http://orcid.org/0000-0003-1680-5252
Maqusood Ahamed http://orcid.org/0000-0001-6025-1950
Mohsin Ali Khan http://orcid.org/0000-0003-0748-3298

References

Ahmad, R. (2019, Jan). Steroidal glycoalkaloids from Solanum nigrum target cytoskeletal proteins: An in silico analysis. PeerJ., *7*, e6012. https://doi.org/10.7717/peerj.6012

Ahmad, S., Abbasi, H. W., Shahid, S., Gul, S., & Abbasi, S. W. (2020, June). Molecular Docking, Simulation and MM-PBSA Studies of Nigella Sativa Compounds: A Computational Quest to identify Potential Natural Antiviral for COVID-19 Treatment. *Journal of Biomolecular Structure and Dynamics*, 1–9. https://doi.org/10.1080/07391102.2020.1775129

Ahmad, A., Husain, A., Mujeeb, M., Khan, S. A., Najmi, A. K., Siddique, N. A., Damanhouri, Z. A., & Anwar, F. (2013, May). A review on therapeutic potential of Nigella sativa: A miracle herb. *Asian Pacific Journal of Tropical Biomedicine*, *3*(5), 337–352. https://doi.org/10.1016/S2221-1691(13)60075-1

Ahmad, R., Khan, M. A., Srivastava, A. N., Gupta, A., Srivastava, A., Jafri, T. R., Siddiqui, Z., Chaubey, S., Khan, T., & Srivastava, A. K. (2020, Jan). Anticancer Potential of Dietary Natural Products: A Comprehensive Review. *Anti-Cancer Agents in Medicinal Chemistry*, *20*(2), 122–236. https://doi.org/10.2174/1871520619666191015103712

Ahmad, Z, Ghafoor, A., & Aslam, M. (2004, May). Nigella sativa–A potential commodity in crop diversification traditionally used in healthcare. *Project on Introduction of Medicinal Herb and Species as Crop. Ministry of Food, Agriculture and Livestock, Pakistan*, *2*, 6–10.

Báez-Santos, Y. M., John, S. E., & Mesecar, A. D. (2015, Mar). The SARS-coronavirus papain-like protease: Structure, function and inhibition by designed antiviral compounds. *Antiviral Research*, *115*, 21–38. https://doi.org/10.1016/j.antiviral.2014.12.015

Bahar, I., Lezon, T. R., Bakan, A., & Shrivastava, I. H. (2010). Normal mode analysis of biomolecular structures: Functional mechanisms of membrane proteins. *Chemical Reviews*, *110*(3), 1463–1497. https://doi.org/10.1021/cr900095e

Caly, L., Druce, J. D., Catton, M. G., Jans, D. A., & Wagstaff, K. M. (2020, April). The FDA-approved drug ivermectin inhibits the replication of SARS-CoV-2 in vitro. *Antiviral Research*, *178*, 104787. https://doi.org/10.1016/j.antiviral.2020.104787

Chang, C. K., Hou, M. H., Chang, C. F., Hsiao, C. D., & Huang, T. H. (2014, Mar). The SARS coronavirus nucleocapsid protein-forms and functions. *Antiviral Research*, *103*, 39–50. https://doi.org/10.1016/j.antiviral.2013.12.009

Chang, C. K., Lo, S. C., Wang, Y. S., & Hou, M. H. (2016). Recent insights into the development of therapeutics against coronavirus diseases by targeting N protein. *Drug Discovery Today*, *21*(4), 562–572. Apr 1https://doi.org/10.1016/j.drudis.2015.11.015

Choudhary, R., & Sharma, A. K. (2020, April). Potential use of hydroxychloroquine, ivermectin and azithromycin drugs in fighting COVID-19: Trends, scope and relevance. *New Microbes and New Infections*, *35*, 100684. https://doi.org/10.1016/j.nmni.2020.100684

de Oliveira, M. D., & de Oliveira, K. M. (2020). Comparative Computational Study of SARS-CoV-2 Receptors Antagonists from Already Approved Drugs. *Cep*, *11981*(8), 7.

Delaney, J. S. (2004, May). ESOL: Estimating aqueous solubility directly from molecular structure. *Journal of Chemical Information and Computer Sciences*, *44*(3), 1000–1005. https://doi.org/10.1021/ci034243x

Forouzanfar, F., Bazzaz, B. S., & Hosseinzadeh, H. (2014, Dec). Black cumin (Nigella sativa) and its constituent (thymoquinone): A review on antimicrobial effects. *Iranian Journal of Basic Medical Sciences*, *17*(12), 929–938.

Ghildiyal, R., Prakash, V., Chaudhary, V. K., Gupta, V., & Gabrani, R. (2020). Phytochemicals as Antiviral Agents: Recent Updates. *InPlant-derived Bioactives*. (pp. 279–295). Springer.

Hassan, T. A., Hollander, S., van Lent, L., & Tahoun, A. (2020, April). Firm-level exposure to epidemic diseases: Covid-19, SARS, and H1N1. *National Bureau of Economic Research*. https://doi.org/10.36687/inetwp119

Heidary, F., & Gharebaghi, R. (2020). Ivermectin: A systematic review from antiviral effects to COVID-19 complementary regimen. *The Journal of Antibiotics*, *73*(9), 593–590. Jun 12: https://doi.org/10.1038/s41429-020-0336-z

Hospital, A., Goñi, J. R., Orozco, M., & Gelpí, J. L. (2015). Molecular dynamics simulations: Advances and applications. *Advances and Applications in Bioinformatics and Chemistry : AABC*, *8*, 37–47. https://doi.org/10.2147/AABC.S70333

Khan, T., Ahmad, R., Azad, I., Raza, S., Joshi, S., & Khan, A. R. (2018, Aug). Computer-aided drug design and virtual screening of targeted combinatorial libraries of mixed-ligand transition metal complexes of 2-butanone thiosemicarbazone. *Computational Biology and Chemistry*, *75*, 178–195. https://doi.org/10.1016/j.compbiolchem.2018.05.008

Li, F. (2016, Sep). Structure, function, and evolution of coronavirus spike proteins. *Annual Review of Virology*, *3*(1), 237–261. https://doi.org/10.1146/annurev-virology-110615-042301

Lipinski, C. A. (2004, Dec). Lead- and drug-like compounds: the rule-of-five revolution . *Drug Discovery Today. Technologies*, *1*(4), 337–341. https://doi.org/10.1016/j.ddtec.2004.11.007

Liu, K., Tang, M., Liu, Q., Han, X., Jin, H., Zhu, H., Li, Y., He, L., Ji, H., & Zhou, B. (2020, Mar). Hydroxychloroquine, a less toxic derivative of chloroquine, is effective in inhibiting SARS-CoV-2 infection in vitro. *Cell Discovery*, *6*(1), 1–4. https://doi.org/10.1038/s41421-020-0156-0

Menounos, P., Staphylakis, K., & Gegiou, D. (1986, Jan). The sterols of Nigella sativa seed oil. Phytochemistry, *25*(3), 761–763. https://doi.org/10.1016/0031-9422(86)88046-3

Morris, G. M., Goodsell, D. S., Halliday, R. S., Huey, R., Hart, W. E., Belew, R. K., & Olson, A. J. (1998, Nov). Automated docking using a Lamarckian genetic algorithm and an empirical binding free energy function. *Journal of Computational Chemistry*, *19*(14), 1639–1662. https://doi.org/10.1002/(SICI)1096-987X(19981115)19:14<1639::AID-JCC10>3.0.CO;2-B

Naithani, R., Mehta, R. G., Shukla, D., Chandersekera, S. N., & Moriarty, R. M. (2010). Antiviral activity of phytochemicals: A current perspective. In *Dietary Components and Immune Function*. (pp. 421–468). Humana Press.

Oprea, T. I., Davis, A. M., Teague, S. J., & Leeson, P. D. (2001, Sep). Is there a difference between leads and drugs? A historical perspective. *Journal of Chemical Information and Computer Sciences*, *41*(5), 1308–1315. https://doi.org/10.1021/ci010366a

Pal, M., Berhanu, G., Desalegn, C., & Kandi, V. (2020, Mar). Severe acute respiratory syndrome Coronavirus-2 (SARS-CoV-2): An update. *Cureus*, *12*(3),e7423. https://doi.org/10.7759/cureus.7423

Parasuraman, S. (2011, Apr). Toxicological screening. *Journal of Pharmacology & Pharmacotherapeutics*, *2*(2), 74–79. https://doi.org/10.4103/0976-500X.81895

Patil, S., Hofer, J., Ballester, P. J., Fattakhova, E., DiFlumeri, J., Campbell, A., & Oravic, M. (2020). Drug Repurposing for Covid-19: Discovery of Potential Small-Molecule Inhibitors of Spike Protein-ACE2 Receptor

Interaction Through Virtual Screening and Consensus Scoring. https://doi.org/10.26434/chemrxiv.12482435.v1

Prajapat, M., Sarma, P., Shekhar, N., Avti, P., Sinha, S., Kaur, H., Kumar, S., Bhattacharyya, A., Kumar, H., Bansal, S., & Medhi, B. (2020, Jan). Drug targets for corona virus: A systematic review. *Indian Journal of Pharmacology*, *52*(1), 56–65. https://doi.org/10.4103/ijp.IJP_115_20

Proudfoot, A. E. (2002). Chemokine receptors: Multifaceted therapeutic targets. *Nature Reviews. Immunology*, *2*(2), 106–115. Febhttps://doi.org/10.1038/nri722

Rebeaud, M. E., & Zores, F. (2020, Apr). SARS-CoV-2 and the Use of Chloroquine as an Antiviral Treatment. *Frontiers in Medicine*, *7*, 184. https://doi.org/10.3389/fmed.2020.00184

Riou, J., & Althaus, C. L. (2020, Jan). Pattern of early human-to-human transmission of Wuhan 2019 novel coronavirus (2019-nCoV), December 2019 to January 2020. Eurosurveillance, *25*(4), 2000058. https://doi.org/10.2807/1560-7917.ES.2020.25.4.2000058

Salem, M. L., & Hossain, M. S. (2000, Sep). Protective effect of black seed oil from Nigella sativa against murine cytomegalovirus infection. *International Journal of Immunopharmacology*, *22*(9), 729–740. https://doi.org/10.1016/S0192-0561(00)00036-9

Tian, S., Wang, J., Li, Y., Li, D., Xu, L., & Hou, T. (2015, Jun). The application of in silico drug-likeness predictions in pharmaceutical research. Adv Drug Deliv Rev, *86*, 2–10. https://doi.org/10.1016/j.addr.2015.01.009

Touret, F., & de Lamballerie, X. (2020, Mar). Of chloroquine and COVID-19. *Antiviral Research*, *177*, 104762. https://doi.org/10.1016/j.antiviral.2020.104762

Trott, O., & Olson, A. J. (2010, Jan). AutoDock Vina: Improving the speed and accuracy of docking with a new scoring function, efficient optimization, and multithreading. *Journal of Computational Chemistry*, *31*(2), 455–461. https://doi.org/10.1002/jcc.21334

Walls, A. C., Park, Y. J., Tortorici, M. A., Wall, A., McGuire, A. T., & Veesler, D. (2020, Mar). Structure, function, and antigenicity of the SARS-CoV-2 spike glycoprotein. Cell, *181*(2), 281–292.e6. https://doi.org/10.1016/j.cell.2020.02.058

Yang, J. M., & Chen, C. C. (2004, May). GEMDOCK: a generic evolutionary method for molecular docking. Proteins, *55*(2), 288–304. https://doi.org/10.1002/prot.20035

Yang, W., Chen, X., Li, Y., Guo, S., Wang, Z., & Yu, X. (2020, Mar). Advances in Pharmacological Activities of Terpenoids. *Natural Product Communications*, *15*(3), 1934578X2090355. https://doi.org/10.1177/1934578X20903555

Yang, J. F., Wang, F., Chen, Y. Z., Hao, G. F., & Yang, G. F. (2019, Dec). LARMD: Integration of bioinformatic resources to profile ligand-driven protein dynamics with a case on the activation of estrogen receptor. *Briefings in Bioinformatics*, *21*(6), 2206-2218. https://doi.org/10.1093/bib/bbz141

Yarnell, E., & Abascal, K. (2011, Apr). Nigella sativa: Holy herb of the middle East. *Alternative and Complementary Therapies*, *17*(2), 99–105. https://doi.org/10.1089/act.2011.17203

Yimer, E. M., Tuem, K. B., Karim, A., Ur-Rehman, N., & Anwar, F. (2019, May). Nigella sativa L.(black cumin): a promising natural remedy for wide range of illnesses. *Evidence-Based Complementary and Alternative Medicine : eCAM*, *2019*, 1528635. https://doi.org/10.1155/2019/1528635